A bidirectional network for appetite control in zebrafish

***Caroline Lei Wee[1,2,5], *Erin Yue Song[1]**, Robert Evan Johnson[1,2], Deepak Ailani[3], Owen Randlett[1], Jiyoon Kim[1], Maxim Nikitchenko[1], Armin Bahl[1], Chao-Tsung Yang[4], Misha Ahrens[4], Koichi Kawakami[3], Florian Engert[1] and **Samuel Kunes[1]**

***Equal contribution first authors**

[1]Department of Molecular and Cell Biology, Harvard University, Cambridge, MA, USA

[2]Program in Neuroscience, Harvard University, Boston, MA, USA

[3]Division of Molecular and Developmental Biology, National Institute of Genetics, Department of Genetics, SOKENDAI (The Graduate University for Advanced Studies), Mishima, Shizuoka, Japan

[4]Howard Hughes Medical Institute, Janelia Farm Research Campus, Ashburn, Virginia, USA.

[5]Institute of Molecular and Cell Biology, A*STAR, Singapore

ABSTRACT

Medial and lateral hypothalamic loci are known to suppress and enhance appetite, respectively, but their interactions and dynamics have not yet been explored. Here we report that, in zebrafish, serotonergic neurons of the ventromedial caudal hypothalamus (cH) become increasingly active during food deprivation, whereas activity in the lateral hypothalamus (LH) is reduced. Exposure to food sensory and consummatory cues reverses the activity states of these two nuclei, reflecting an opposing internal hunger state induced by food. An intermediate activity state is restored as satiety approaches. The overall antagonistic relationship of cH and LH was confirmed by simultaneous calcium imaging, and a causal relationship was established by targeted stimulation and ablation of the cH. The collective data allows us to propose a model in which activities in anti-correlated hypothalamic nuclei direct distinct phases of hunger, and thus coordinate energy balance via mutually antagonistic control of distinct behavioral outputs.

INTRODUCTION

The regulated intake of food based on caloric needs is a fundamental homeostatically controlled process that is essential for health and survival. The hypothalamus is a highly conserved central convergence point for the regulation of the neural and biochemical pathways underlying these basic mechanisms. Early studies demonstrated by way of electrical stimulation or lesions that specific hypothalamic regions play important roles in the regulation of appetite. For example, while stimulation of ventromedial hypothalamic loci in rodents and cats reduced feeding, activation of more lateral hypothalamic loci increased both hunting behavior and food intake (ANAND and BROBECK, 1951; BROBECK et al., 1956; DELGADO and ANAND, 1953; Krasne, 1962). Conversely, lateral hypothalamic lesions were found to reduce feeding to the point of starvation, whereas medial hypothalamic lesions resulted in overeating(ANAND and BROBECK, 1951; Hoebel, 1965; TEITELBAUM and EPSTEIN, 1962). Thus, the lateral and medial hypothalamic regions came to be regarded as “hunger” and “satiety” centers, respectively.

Recent experiments employing optical and electrophysiological methods have lent support to expectations based on these early studies. For example, GABAergic neurons in the lateral hypothalamus were observed to be activated during feeding and essential for enhanced food intake during hunger (Jennings et al., 2015; Stuber and Wise, 2016). However, these experiments have examined only subsets of hypothalamic neurons; their activity patterns in the context of the entire network remain unknown. This limited view hampers our understanding of the dynamical interactions between the ensemble of brain circuits thought to be important for the initiation, maintenance and termination of food consumption (Sternson and Eiselt, 2017).

Here, we leverage the small and optically accessible larval zebrafish to identify modulatory regions central to the control of appetite and to shed light on their specific roles and dynamical activity patterns in relation to the whole brain and behavior. Using pERK-based brain-wide activity mapping we first identified neuronal populations that display differential neural activity under conditions of hunger and satiety. We show that lateral and medial hypothalamic

regions have anti-correlated activity patterns during hunger, voracious feeding and satiety. Next, through a combination of calcium imaging, optogenetics and ablation analysis, we show that serotonergic neurons in the caudal periventricular zone of the medial hypothalamus (cH) are state-dependent regulators of feeding behavior, likely via their modulation of the lateral hypothalamus. This allows us to propose a model where mutually antagonistic brain states regulate energy balance by encoding distinct signals in different facets of appetite control.

RESULTS

Whole brain activity mapping of appetite-regulating regions

Larval zebrafish hunt their prey, paramecia, through a sequence of motor actions that has been considered a hardwired reflex response to external prey stimuli (Bianco et al., 2011; Semmelhack et al., 2015; Trivedi and Bollmann, 2013). Only recently has evidence emerged that this behavior is flexibly modulated by satiation state (Filosa et al., 2016; Jordi et al., 2015, 2018) and that larvae at 7 **d**ays **p**ost-**f**ertilization (dpf) display enhanced hunting and enhanced food intake after a period of food deprivation. A robust readout of food intake in larval zebrafish was obtained both by fluorescently-labeled paramecia and behavioral analysis approaches that have been adapted for this study (Johnson et al., 2019; Jordi et al., 2015, 2018; Shimada et al., 2012). Given that a 2-hour period of food-deprivation is sufficient to robustly enhance subsequent food intake, fish at the end of this food-deprivation period are considered to be in a state of “hunger” and nutrient/caloric deficit. Indeed, up to 15 min after food-presentation, such food-deprived animals display a strong upregulation of hunting and food intake relative to fish with continuous access to food (fed fish). As the fish in this state are likely still in a caloric/nutrient deficit and display enhanced food intake, we will refer to this phase as “voracious feeding”. Finally, as the fish continue to consume food, their rate of food intake declines to a low level comparable to that of fed fish. As we describe below, this state of continuous low level feeding in the presence of ample food sources reflects a state of “satiety”

that is the same or similar to that of a continuously fed animal.

As a first step toward understanding the homeostatic control of feeding in this simple vertebrate system, we employed whole-brain neuronal activity mapping via phosphorylated ERK visualization in post-fixed animals (MAP-mapping; Randlett et al., 2015). Whole brain confocal image datasets of phospho-ERK expression were gathered from animals sacrificed after 15 minutes of voracious feeding that followed a 2-hour period of food deprivation. For comparison, image sets were also gathered from animals that had been fed constantly. These image volumes were registered to a standardized brain atlas and are displayed as a difference map (Figure 1b), revealing significant differences in neural activity when comparing voracious feeding with constant feeding (Figure 1b-d, Video 1, Supplementary Tables 1-2). Since both experimental groups experienced similar sensory stimuli (i.e. exposure to the same concentration of paramecia), differences in brain activity should reflect the animal's internal hunger state, which could also manifest as an enhanced sensitivity to food cues, and/or enhanced hunting and prey capture. Indeed, multiple sensorimotor loci related to hunting showed enhanced activity in the food-deprived state. These included stronger activation in retinal Arborization Fields (AFs; optic tectum and AF7), pretectum, as well as downstream hindbrain loci, such as reticulospinal and oculomotor neurons that all have been shown to be engaged during prey capture behavior (Bianco and Engert, 2015; Muto et al., 2017; Semmelhack et al., 2015). In addition, enhanced activity was observed in the cerebellum, inferior olive, vagal sensory and motor neurons, area postrema and locus coeruleus, all of which have been implicated in producing motor programs related to feeding behavior (Ahima and Antwi, 2008; Ammar et al., 2001; Dockray, 2009; Zhu and Wang, 2008).

We next focused our attention on brain areas likely to be involved in regulating internal states related to hunger and satiety. These included an area of particularly strong differential activity in the lateral region of the intermediate hypothalamus (LH; Fig. 1b-d), which has recently been identified as part of the feeding pathway in larval zebrafish (Muto et al., 2017), and whose

mammalian analog has been strongly implicated in appetite control (Sternson and Eiselt, 2017). However, the zebrafish LH, unlike its mammalian counterpart, does not express melanin-concentrating hormone (MCH) or contain orexin (hypocretin)-positive neurons, nor does it clearly express other major feeding-related peptides (Figure 1- Figure Supplement 1 and 2). MCH, hypocretin and other appetite-related neuromodulators (AgRP, MSH, CART, NPY) are in fact expressed in other nearby areas of the hypothalamus (Figure 1 - Figure Supplement 1). The zebrafish LH region does however contain a variety of glutamatergic and GABAergic cell types (Figure 1 - Figure Supplement 2) that have been shown to be important for regulation of feeding in mammals, independent of MCH and orexin (Jennings et al., 2015; Stuber and Wise, 2016). Among areas that showed relatively decreased neural activity upon feeding food-deprived animals, the most significant was the caudal hypothalamus (cH), which contains monoaminergic (mainly serotonergic and dopaminergic) neurons (Fig 1c; Kaslin and Panula, 2001; Lillesaar, 2011). Indeed, in all of nine independent MAP-mapping experiments, activity was reduced in the cH and increased in the LH within 15 min of food presentation (Fig 1c). The evident inverse relationship between overall LH and cH activity in this context was supported by independent component analysis (Randlett et al., 2015), which was applied to all feeding-related MAP-mapping data, and uncovered multiple components where the cH and LH are strongly anti-correlated (Figure 1e, Figure 1 - Figure Supplement 3). These results led us to hypothesize that the lateral and caudal hypothalamus may form a functionally interconnected network with opposing activity patterns.

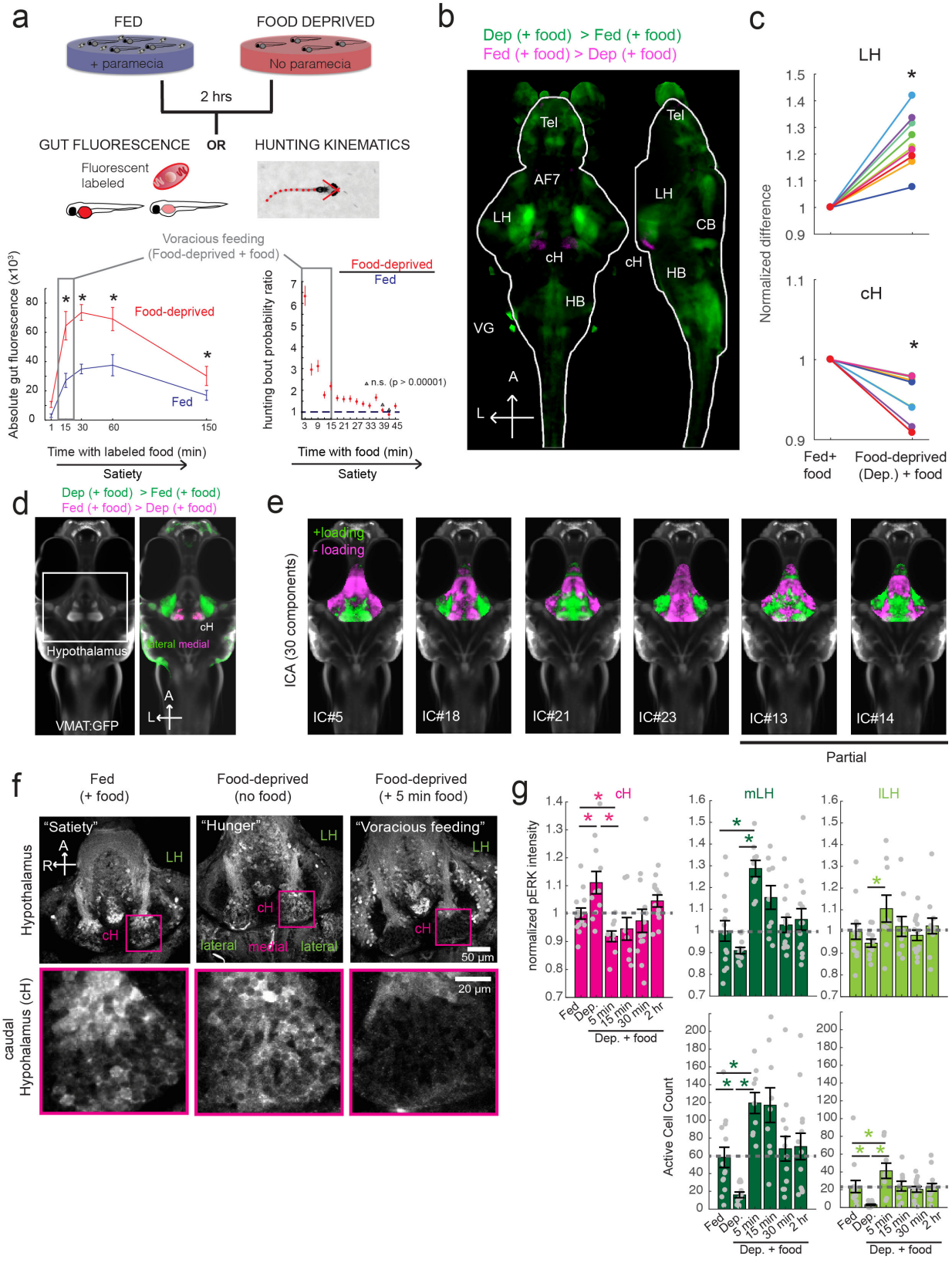

Figure 1 with 4 supplements: Whole brain activity mapping reveals anti-correlated hypothalamic clusters

(a) Top: Schematic of protocols used to evaluate appetite behavior in larval zebrafish. At 7 or 8 dpf, larvae were either food-deprived for 2 hours, or fed with excess paramecia for this duration. After 2 hrs (2-4 hours in the case of behavioral imaging), they were subject to a quick wash, followed either by: 1) addition of excess fluorescent-labeled paramecia (left), 2) high-resolution behavioral imaging (right). **Bottom left:** Gut fluorescence measurements of food-deprived (red) or fed (blue) fish as a function of feeding duration. Groups of fed or food-deprived larvae were fixed at indicated time points after feeding of labeled paramecia (fed: n=7/18/19/17/17, food-deprived: n= 8/23/20/14/15). Food-deprived fish had significantly higher gut fluorescence than fed fish overall ($p = 7.5859x10^{-10}$, Two-way ANOVA, asterisk indicates corrected p-values<0.05. **Bottom right:** The probability of performing a hunting-related swim bout across fed and food-deprived fish groups in 3-minute time bins over 45 minutes. Error bars represent 90% confidence intervals. For all bins except those indicated with triangles, the null hypothesis that initial feeding condition has no effect on hunting-bout probability is rejected ($p < 0.00001$, Fisher's Exact Test comparing binomial probability distributions per bin). Fed: n =85655 bouts from 73 fish; Food-deprived n = 75357 bouts from 57 fish. Since the rate of food intake and hunting behavior was highest in the first 15 minutes (voracious feeding phase, gray boxes), we chose this time point for subsequent MAP-mapping experiments.

(b) Brain-wide activity mapping of food-deprived (Dep.) and fed fish, in response to food. Data from 9 experiments (n = 557 fish total) were combined to generate this map. Activated regions include the telencephalon (Tel), Arborization field 7 (AF7), cerebellum (CB), hindbrain (HB), Vagal ganglion (VG) and lateral lobe of the intermediate hypothalamus (LH). Suppression was observed in the caudal hypothalamus (cH) and some parts of the telencephalon. Scale bar = 100 μm. Also see Video 1.

(c) ROI-specific analysis of LH and cH regions in 9 independent MAP-mapping experiments (20-30 fish per treatment per experiment). Food-deprived fish constantly had higher LH and lower cH activity in response to food ($p=0.0039$ for both cH and LH, Wilcoxon Signed Rank Test).

(d) Z-projection of same MAP-map showing the hypothalamus, where lateral regions (i.e. LH) are strongly activated and medial regions (e.g. cH) are suppressed. The map is overlaid on an anatomy stack for the transgenic line *Tg(etVMAT:GFP)* to highlight the location of cH neurons.

(e) Six examples of independent component analysis (ICA) maps. Voxels for each recovered independent component (IC) are shown as maximum projections, with intensity proportional to the z-score of the loadings of the ICA signal. These ICs, along with others (16/30) highlight LH and cH regions of opposite loadings, suggesting they may be part of a network with anti-correlated activity patterns. Positive (+) loading and Negative (-ve) loadings are reflected in green and magenta respectively.

(f) Higher resolution imaging of dissected brains stained with pERK during phases of feeding. Scale bar: 50 μm. Inset: Higher magnification view of cH neurons. Scale bar: Scale bar = 20 μm. Fish were mounted ventral side up.

(g) Quantification of cH activity (normalized pERK fluorescence) and LH (medial LH and lateral LH) activity (normalized pERK fluorescence) (top) and # pERK-positive cells (bottom) in fed and food-deprived fish (n =13/11/9/9/13/12).

Normalized pERK intensity (cH/mLH/lLH): Fed vs Dep. (p = 0.016/0.17/0.17), Dep. vs Dep + 5 min food ($p=3.1x10^{-4}$/$9.9x10^{-5}$/0.02), Fed vs Dep. + 5 min food (p= 0.0097/0.001/0.08).

Active Cell count (mLH/lLH): Fed vs Dep. (p = 0.001/0.0038), Dep. vs Dep + 5 min food ($p= 9.7x10^{-5}$/$1.3x10^{-5}$), Fed vs Dep. + 5 min food (p= 0.0038/0.048). Asterisks denote p<0.05, one-tail Wilcoxon Rank Sum Test. Note that mean pERK intensity does not change as significantly as active cell count.

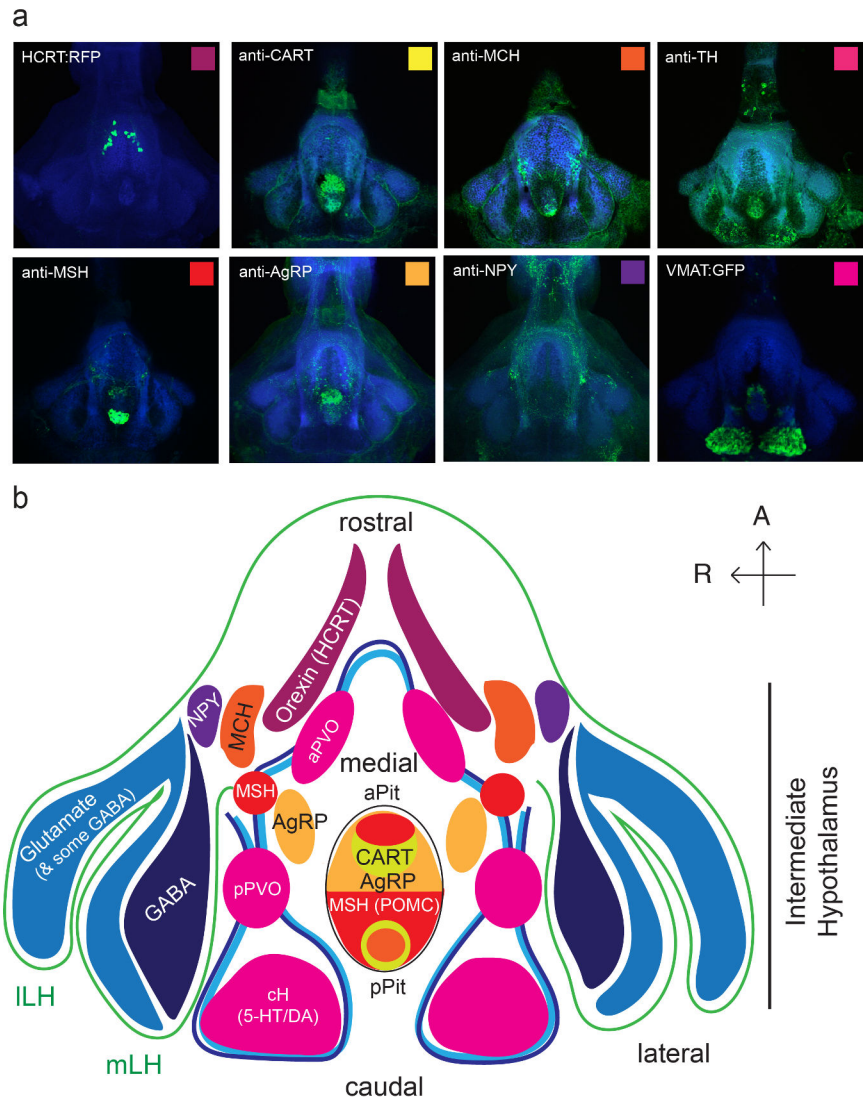

Figure 1 - Figure Supplement 1: Anatomical characterization of intermediate hypothalamus feeding areas

(a) Expression patterns of a number of feeding-related peptides in the zebrafish hypothalamus, based on antibody-staining or transgenic labels. HCRT = hypocretin (orexin), CART = cocaine and amphetamine related transcript MCH = melanin-concentrating hormone, TH = tyrosine hydroxylase (labels dopaminergic and/or noradrenergic neurons), MSH = alpha-melanocyte stimulating hormone, AgRP = Agouti-related peptide, NPY = neuropeptide Y, VMAT = vesicular monoamine transporter (labels dopaminergic (DA) and serotonergic neurons (5-HT)). Note that MCH and HCRT staining is absent from the zebrafish LH. Though not apparent from the schematic, HCRT is located more dorsally. The preoptic area, which contains oxytocinergic as well as other peptidergic neurons, is located more dorsally and not reflected in this schematic.

(b) Schematic summarizing zebrafish hypothalamic peptide expression. GABA (dark blue) and glutamatergic (blue) neurons are found in the lateral hypothalamus (see Figure 1- Figure Supplement 2) and also throughout the medial regions of the hypothalamus. PVO = paraventricular organ, which also contains DA and 5-HT neurons. A number of peptidergic neurons are located within the anterior and posterior pituitary/hypophysis (aPit and pPit). Color code corresponds to images in (a). A = anterior, R = right.

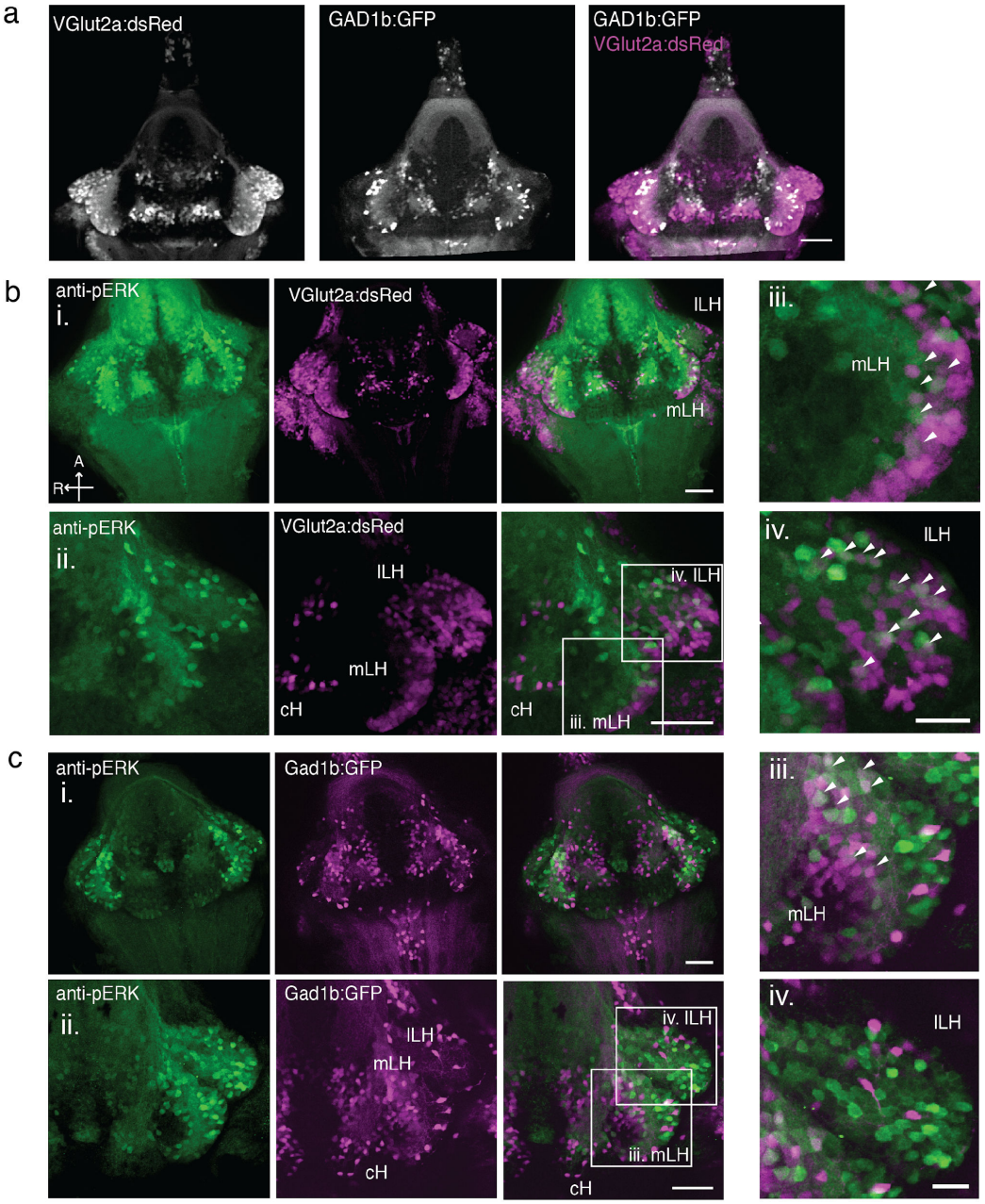

Figure 1- Figure Supplement 2: Characterization of zebrafish LH

(a) Glutamatergic and GABAergic neuron distribution in the hypothalamus. *Tg(VGlut2a:dsRed)* and *Tg(GAD1b:GFP)* transgenic fish were dissected, imaged and registered onto a common reference hypothalamus.

(b) Glutamatergic cells, labeled by *Tg(VGlut2a:dsRed)*, overlap with active (pERK-positive) neurons in both the lLH and outer rim of the mLH. (i) Overview of hypothalamus. (ii) Higher magnification images of LH. (iii-iv) Inset showing overlap of lLH and outer rim of mLH with glutamatergic cells.

(**c)** GABAergic cells, labeled by *Tg(Gad1b:GFP),* overlap with active neurons in the inner rim of the mLH but not the lLH. (i) Overview of hypothalamus. (ii) Higher magnification images of LH. (iii-iv) Inset showing overlap of inner rim of mLH with GABAergic cells. White arrows point to examples of overlapping cells. All fish were mounted ventral side up. Scale bar = 50 μm. Inset scale bar = 20 μm.

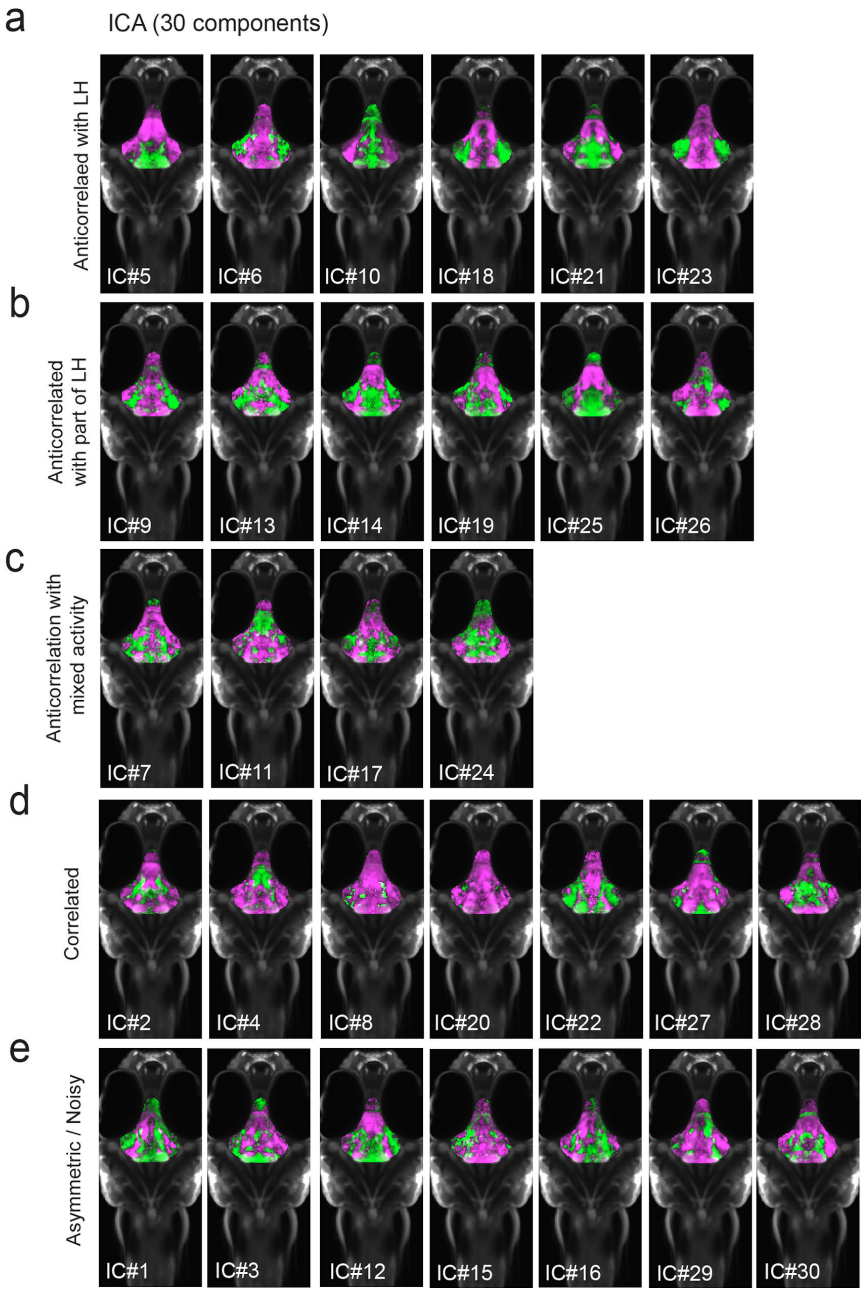

Figure 1- Figure Supplement 3: All 30 independent components extracted from ICA analysis. This method separates pERK signals into statistically independent components based on their correlated activity, thus identifying putative functional connectivity (both positive or negative relationships) between different brain regions (Randlett et al., 2015; see Methods). To increase the robustness of the analysis, we included fish from other feeding-related treatments that we did not otherwise use in this manuscript (n = 904 fish total).

(a-c) From this analysis, we identified multiple independent component networks (ICs) in which at least part of the LH displayed an inverse activity relationship (i.e. opposite loadings) with the cH (16/30).

(d) 7/30 ICs had correlated LH and cH activity.

(e) The other 7/30 had asymmetrical or noisy activity patterns.

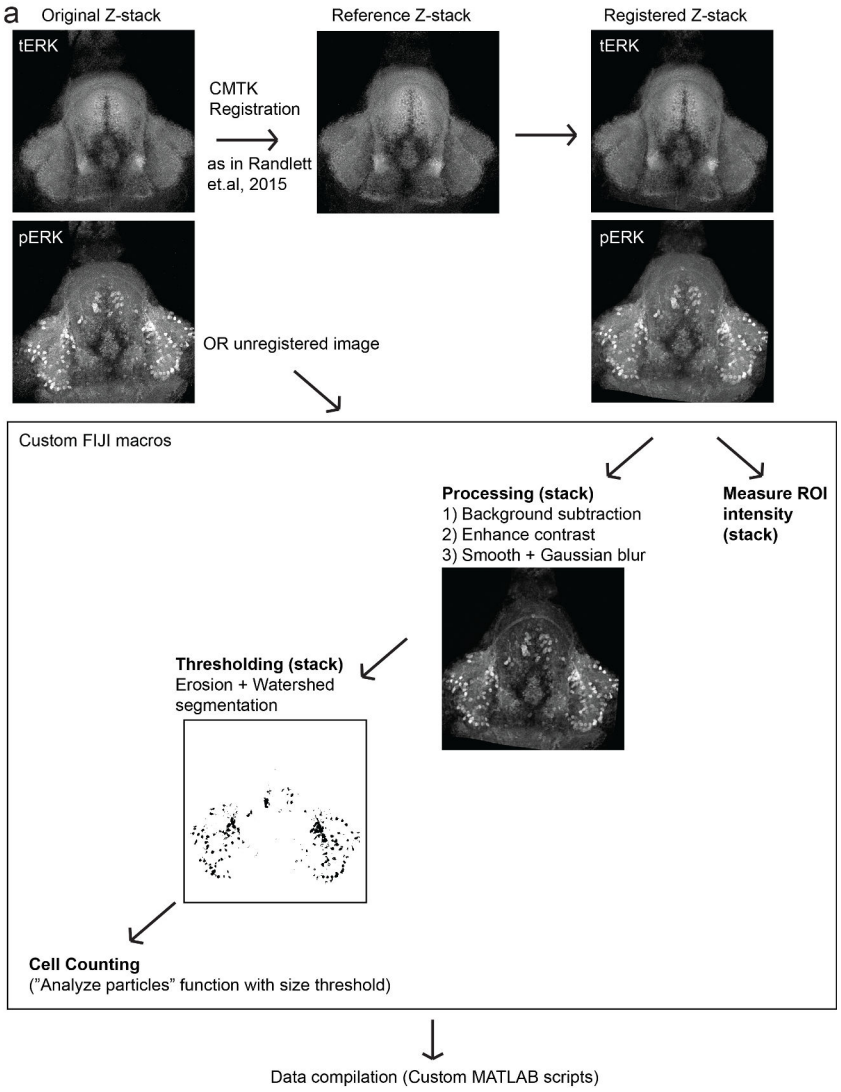

Figure 1 – Figure supplement 4: Automated quantification of pERK-positive cells

(a) Method by which we quantify pERK-positive ("active") cell count in a high-throughput manner. This method works best with high-resolution images (i.e. dissected brains). Brain stacks are registered onto a reference brain within the same dataset, using the tERK channel, though there is the option of using unregistered images (for which individual ROIs have to be defined for each image). A series of processing steps allows for automated segmentation of pERK-positive cells using the same manually optimized threshold across the entire dataset.

Cellular dissection of hypothalamus neural activity reveals modulation by satiation state

To probe neural activity changes with higher resolution, we performed pERK staining in dissected brains, and examined the activity of these populations in time course experiments that spanned the period of food-deprivation and subsequent feeding (Figure 1f-g, Figure 2). We

quantified changes in mean cellular fluorescence as well as changes in the number of active cells or cell clusters (Figure 1 - Figure Supplement 4). While the high density of labeled cells and high background fluorescence in the cH made the identification of individual neurons difficult, we found that in the LH segmentation of individual neurons and classifying activity based on the thresholded fluorescence levels provided a cleaner and more reliable readout for overall neuronal activity. Using these respective metrics, we observed that mean fluorescence in the cH was predictably high in food-deprived fish, while the number of active neurons in the medial and lateral lobes of the LH (mLH and lLH, respectively) was low when compared to continuously fed animals. However, within 5 minutes of food presentation, cH activity fell dramatically to a level significantly below that observed in continuously fed fish (Figure 1f). This characteristically low cH activity level was accompanied by a large increase in LH mean fluorescence and neuron activity, which is consistent with our MAP-mapping results. As the feeding period continued, LH neuronal activity declined and, reciprocally, cH activity increased, coincident with the decline in voracious hunting and food ingestion (Figure 1f). After two hours, neural activity in the cH and LH and feeding behavior all converged onto baseline levels similar to those observed in continuously fed fish (Figure 1f). Thus these two neuronal populations display anti-correlated activity patterns over time frames that span the progression of hunger during food-deprivation, voracious feeding and the gradual return to satiety.

Satiation state influences the sensitivity of cH and LH populations to food

The neural activity patterns described above suggest that cH and LH activity may report the satiation state of the animal. To better align these patterns with the animal's internal state, we examined these loci over a time course that started with food removal from well-fed animals, followed by food presentation after a variable food-deprivation period (30 min or 2 hours, Figure 2). We found that food removal resulted in a reduction of the number of active mLH and lLH neurons within 30 minutes. In contrast, cH activity gradually increased, with a significantly higher level of activity occurring between 30 min and 2 hours post-food removal. A possible

253 interpretation of these patterns is that LH activity is directly driven by the presence of food cues
254 (as noted by Muto et al 2017), whereas the level of activity observed in cH neurons is a
255 correlate of the animal's nutrient/caloric deficit and resulting hunger state in the absence of food,
256 possibly even generating the signal necessary to sensitize the LH's responsiveness to such
257 stimuli.

258 Food presentation not only rapidly reverses the activity patterns of both loci, but also
259 does so in a manner correlating with the length of food-deprivation. Indeed, fish that had been
260 food-deprived for longer periods (2-4 hrs) displayed a relatively enhanced induction of LH
261 activity upon the introduction of food. Likewise, the reduction in cH activity on food presentation
262 was significantly more pronounced when it followed a longer period of prior deprivation; both of
263 these neural responses were strongly correlated with enhanced food consumption (voracious
264 feeding; Figure 2, Figure 2 – Figure Supplement 1). As prey continues to be consumed, activity
265 in both loci gradually reverts back to the baseline levels representative for fed animals (Figure
266 1f-g, 2d).

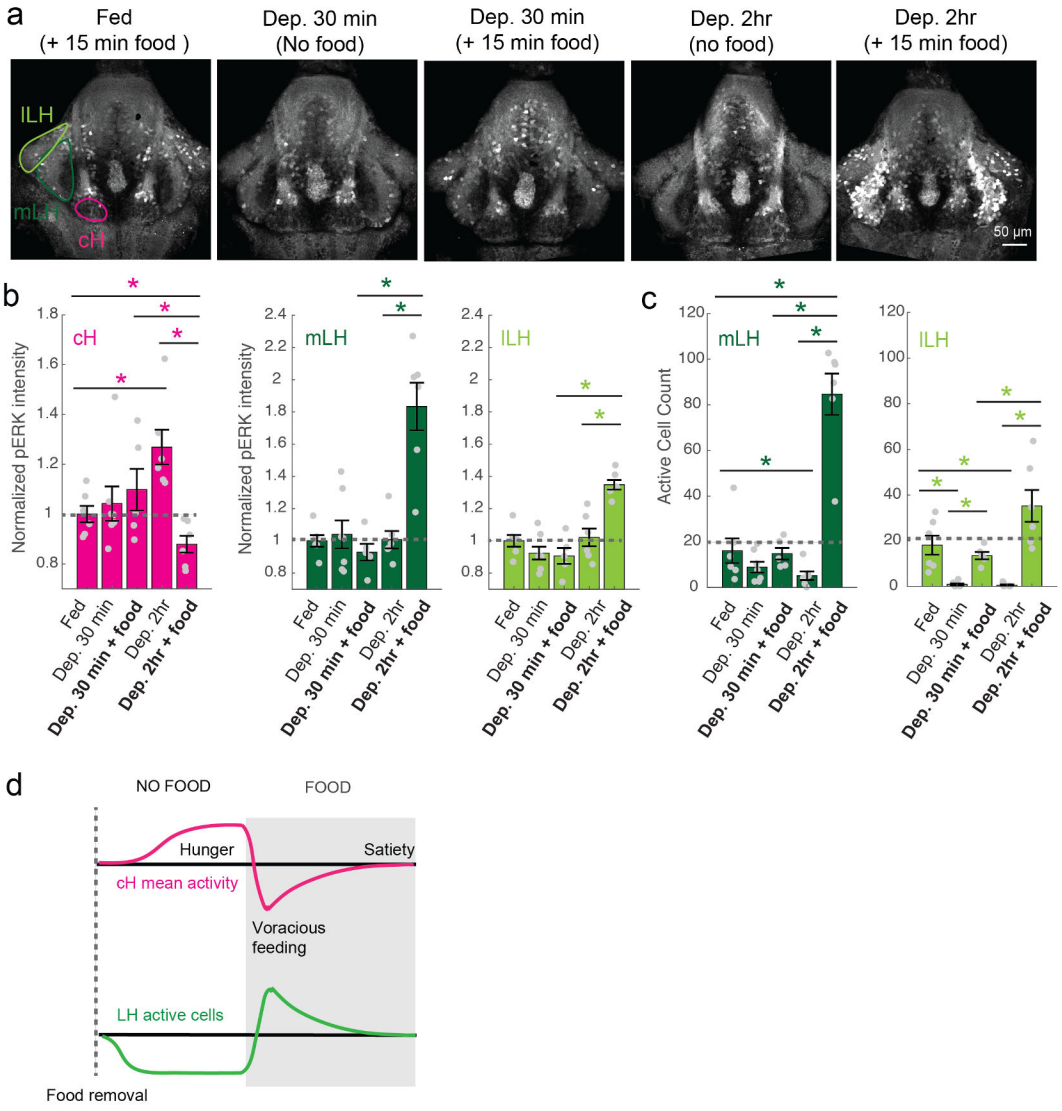

Figure 2 with 5 supplements: cH and LH activities are modulated by food and satiation state

(a) Representative images showing how cH and LH activity in the presence and absence of food vary with the extent of food-deprivation, from the same dataset quantified below.

(b) Normalized pERK intensity in the cH increases with food-deprivation, whereas normalized LH pERK intensity does not change significantly, except during voracious feeding (Dep. 2 hr + food). Normalized pERK intensity (cH/mLH/lLH): Fed vs Dep. 2 hr (p = 0.0022/0.41/0.59), Fed vs Dep. 2 hr + food (0.047/0.0011/0.0011), Dep. 30 min + food vs Dep. 2 hr + food (p = 0.041/0.0022/0.0022), Dep. 2 hr vs Dep. 2 hr + food (p = 0.0022/0.0011/0.0022).

(c) The number of active LH (particularly lLH) cells decline within 30 min of food deprivation, and is significantly enhanced during feeding, particularly after a longer period of food-deprivation. Active cell count (mLH/lLH): Fed vs Dep. 30 min (p = 0.155/5.8x10^{-4}), Fed vs Dep. 2 hr (p = 0.047/0.011), Dep. 30 min + food vs Dep. 2 hr + food (p = 0.0022/0.0043), Dep. 30 min vs Dep. 30 min + food (p = 0.07/0.013), Dep. 2 hr vs Dep. 2 hr + food (p = 0.0011/0.0011), Fed vs Dep. 2 hr + food (p = 0.0022/0.07), n = 6/7/5/6/6 fish, One-tail Wilcoxon Rank Sum Test.

(d) Schematic of inferred cH and LH activity over phases of feeding. LH active cell count appears to decline more rapidly than the rise in cH activity. More supporting data can be found in the supplements.

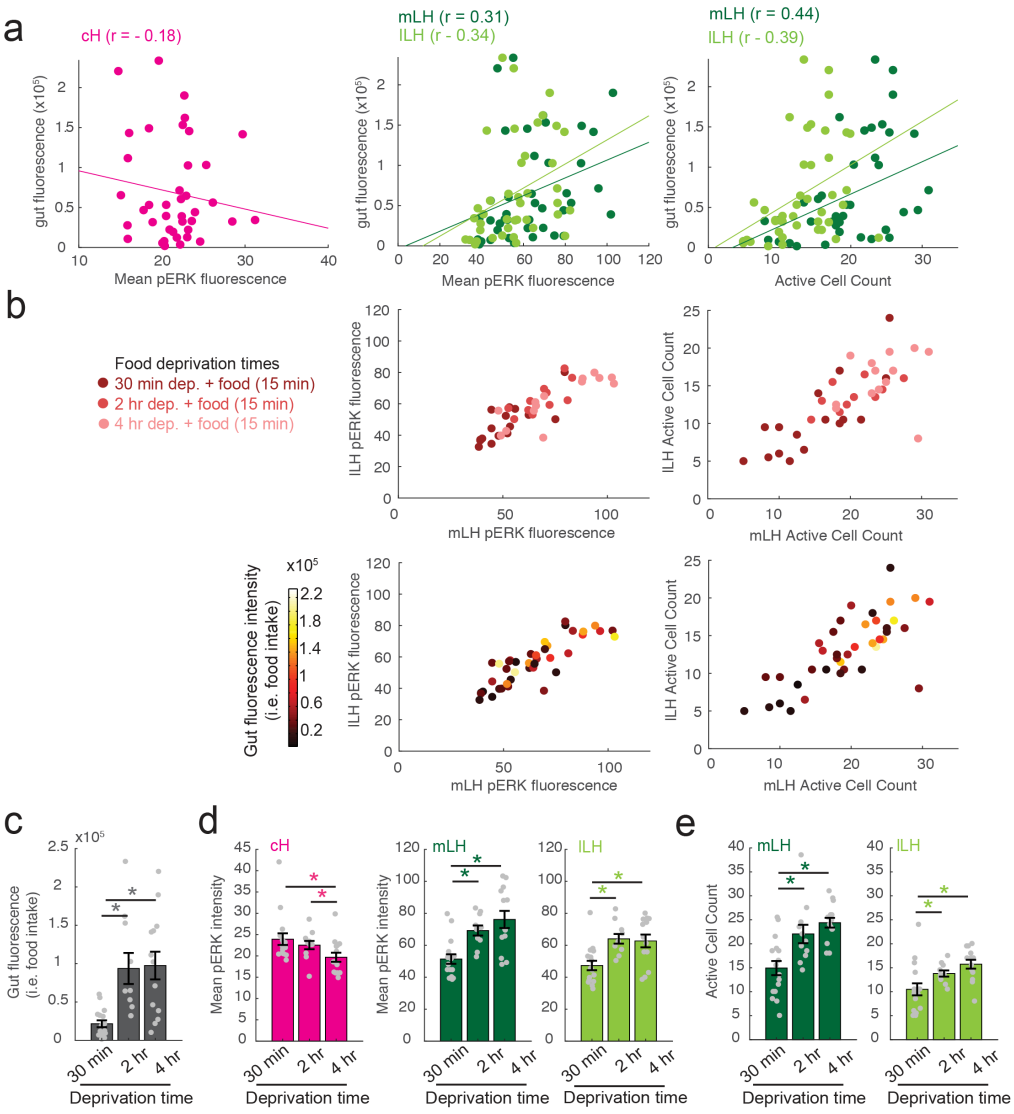

Figure 2 - Figure Supplement 1: Additional data showing modulation of cH and LH by satiation state, and correlation with food intake

(a) Gut fluorescence (i.e. food intake) as a function of mean cH pERK fluorescence, mean LH (mLH and lLH) pERK fluorescence and active cell count. Each datapoint represents a single fish.

(b) Top: mLH and lLH mean pERK fluorescence (left) and active cell count (right) as a function of food-deprivation time (denoted by color intensity). **Bottom:** mLH and lLH mean fluorescence (left) and cell count (right) as a function of gut fluorescence (i.e. food intake) after 15 min of feeding (denoted by color intensity).

(c-e) Quantification of gut fluorescence, cH and LH mean pERK fluorescence and LH active cell count across different food deprivation times (30 min, 2 hr and 4 hr). Note that in this dataset, these fish brains have been stained individually, which may have affected cH quantification.

(c) Food intake: 30 min vs 2 hr dep. ($p = 2.8x10^{-4}$), 30 min vs 4 hr dep. ($p = 4.0x10^{-4}$), 2 hr vs 4 hr dep. ($p = 0.56$). Asterisk denotes $p< 0.05$, n = 16/11/14 fish, One-tail Wilcoxon Rank Sum Test.

(d) Mean pERK fluorescence (cH/mLH/lLH): 30 min vs 2hr dep. ($p = 0.60/0.001/5.9x10^{-4}$), 30 min vs 4 hr dep. ($p=0.084/8.6x10^{-4}/0.058$), 2 hr vs 4 hr dep. ($p =0.02/0.24/0.54$)

(e) Active cell count (mLH/lLH): 30 min vs 2 hr dep. ($p = 0.0073/0.0094$), 30 min vs 4 hr dep. ($p= 1.6x10^{-4}/0.0017$), 2 hr vs 4 hr dep. ($p = 0.056/0.053$).

Given the indirect nature of activity mapping in post-fixed animals, as above, we employed *in vivo* calcium imaging to measure cH and LH neuronal activities during food deprivation in real time (Figure 2 - Figure Supplement 3-5). Two transgenic Gal4 drivers, *Tg(116A:Gal4)* and *Tg(76A:Gal4)*, were used to drive expression of GCaMP6s (*Tg(UAS:GCaMP6s)*) in large subsets of cH and LH neurons (Figure 2 - Figure Supplement 2-3). The 116A:Gal4 transgene drives expression mainly in serotonergic neurons in the cH (88.9±0.8% 5-HT positive) and paraventricular organ (PVO; Figure 2- Figure Supplement 2), whereas 76A:Gal4 drives expression in a large proportion of LH cells (Figure 2 - Figure Supplement 3, Muto et al., 2017). Consistent with our pERK results, the initial calcium-mediated mean fluorescence and firing frequency of a subset of cH neurons scaled with the length of food-deprivation prior to imaging (Figure 2- Figure Supplement 3d), and increased further as food-deprivation continued over the 2 hr imaging period (Figure 2 - Figure Supplement 3-5). The largest rate of increase occurred during the initial hour of food-deprivation (Figure 2 - Figure Supplement 3-5).

Analysis of LH activity gave more diverse results over the course of the food-deprivation time course. While some mLH and lLH voxels showed a predicted reduction in baseline fluorescence and firing rate, many others displayed a significant enhancement of baseline activity. It is possible that these changes reflect real dynamics in certain cellular or neuropil subtypes within the LH, or that they are artifacts of head fixation. Despite the significant diversity in response properties within the LH, we still observe, in line with our expectations, an overall negative correlation of lLH calcium spikes with the mean value of cH fluorescence (Figure 2 - Figure Supplement 4 and 5).

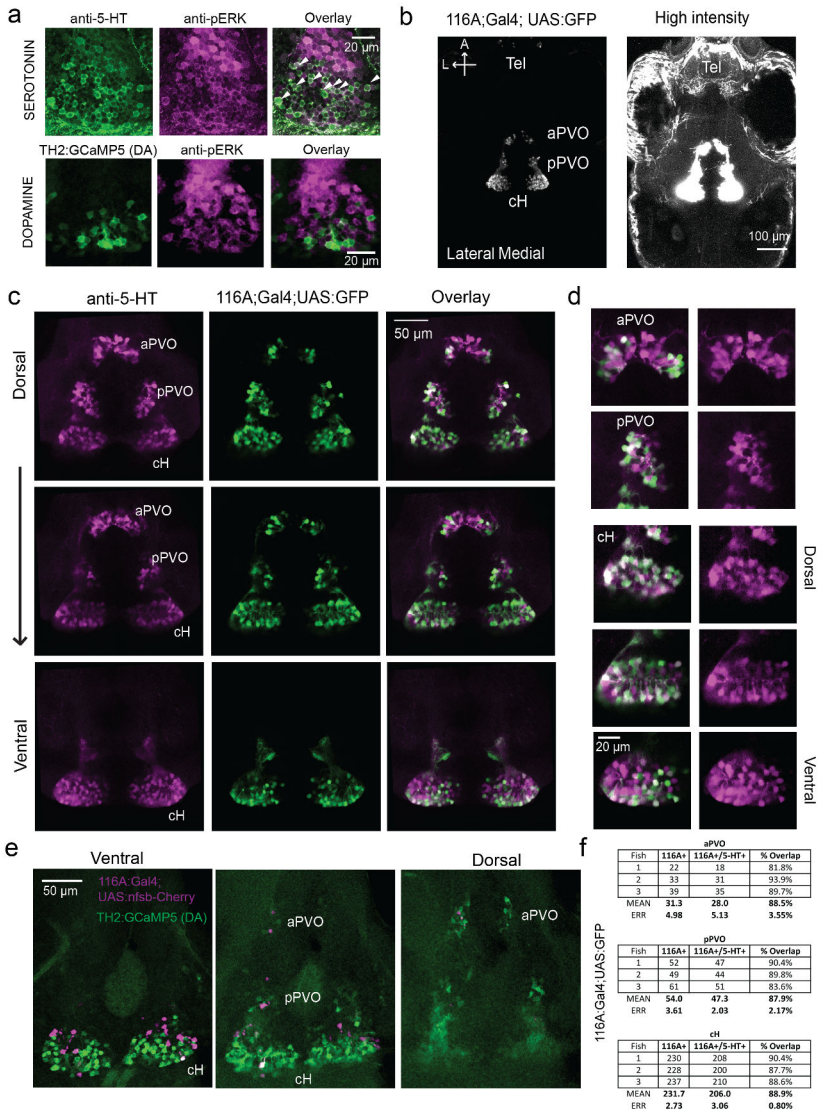

Figure 2 - Figure Supplement 2: Characterization of the cH and 116A:Gal4 line

(a) pERK-positive cH cells overlaps with anti-5-HT immunostaining and *Tg(116A:Gal4)* cells, and less with *Tg(TH2:GCaMP5)* (i.e. dopaminergic) cells. Scale bar = 20µm. White arrows point to examples of overlapping cells.

(b) Z-projection images of whole mount *Tg(116A:Gal4;UAS:GFP)* fish at low (left) and high (right) intensities. Scale bar = 100 µm.

(c) Overlap of *Tg(116A:Gal4;UAS:GFP)* with anti-5-HT immunostaining is seen in all layers of the caudal hypothalamus, and also the anterior and posterior paraventricular organ (aPVO and pPVO). Each row shows a different Z-plane, moving from more dorsal to more ventral. Scale bar = 50 µm.

(d) Higher magnification images of cH, aPVO and pPVO from left side of image in **(c).**

(e) Minimal overlap of *Tg(116A:Gal4;UAS:nfsb-mCherry)* with dopamine neurons labeled by *Tg(TH2:GCaMP5).* Note that the *Tg(116A:Gal4;UAS:nfsb-mCherry)* transgenic, which is used in ablation experiments, shows sparser labeling than with *Tg(UAS:GFP).* Scale bar = 50 µm.

(f) Quantification of 5-HT overlap with *Tg(116A:Gal4;UAS:GFP)* in the cH, aPVO and pPVO.

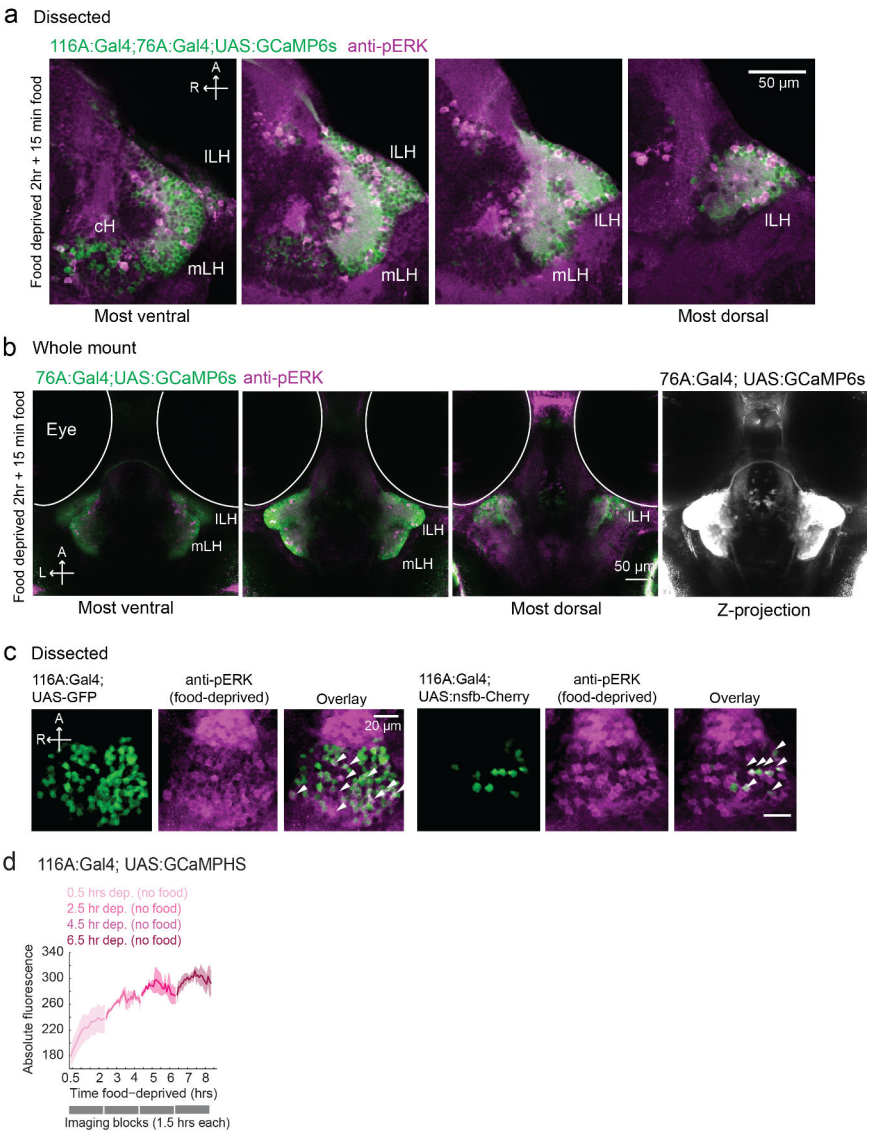

Figure 2 - Figure Supplement 3: 116A and 76A:Gal4 expression overlap with pERK activity

(a) mLH and lLH activity in voraciously-feeding fish overlaps with *Tg(76A:Gal4;UAS:GCaMP6s)* expression (dissected brains). All visible pERK-positive neurons were also co-labeled with GCaMP6s.*Tg(116A:Gal4)* is also epressed. Scale bar = 50 µm.

(b) mLH and lLH activity in voraciously-feeding fish overlaps with *Tg(76A:Gal4;UAS:GCaMP6s)* expression (whole-mount). All visible pERK-positive neurons were also co-labeled with GFP. Note that more dorsally and anteriorly other neurons beyond the LH are labeled. Scale bar = 50 µm.

(c) pERK positive cells (food-deprived fish) overlap partially with *Tg(116A:Gal4)* expression. Left: *Tg(116A:Gal4;UAS:GFP)* Right: *Tg(116A:Gal4;UAS:nfsb-mCherry).* Scale bar = 20 µm.

(d) Mean cH activity *(Tg(116A:Gal4;UAS:GCaMPHS)* increases as a function of food-deprivation time. Larvae were food-deprived for 0.5, 2.5, 4.5 or 6.5 hours (n = 12/4/4/8), quickly embedded in agarose and subsequently imaged for 1.5 hours (every 5 minutes) under a confocal microscope. See Figure 2 - Figure Supplement 4-5 for simultaneous calcium imaging of cH and LH activity at higher temporal resolution.

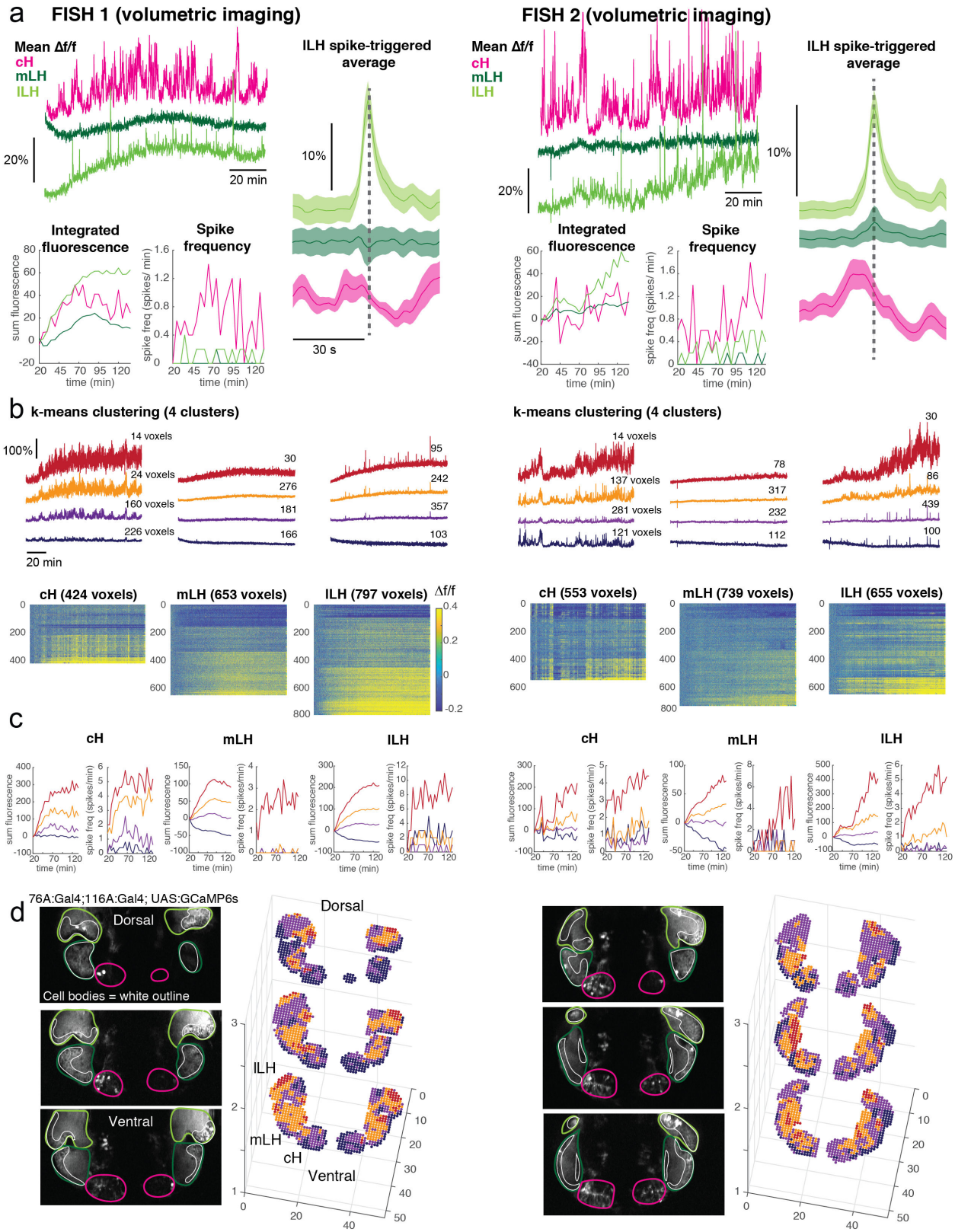

Figure 2 - Figure Supplement 4: Calcium imaging of cH and LH over food-deprivation reveal complex dynamics (volumetric imaging)

(a) Two fish (left and right) are shown. **Top left:** Mean Δf/f across the entire cH, mLH and lLH; **Bottom left:** calcium dynamics (integrated (sum) fluorescence and calcium spike frequency, 5 min bins) over the course of a 2 hr long imaging session. Fish were imaged ~20 min after embedding, thus initial food-deprivation time is 20 min. **Right:** Spike-triggered averages based on lLH calcium spikes reveal an accompanying reduction in cH calcium fluorescence (Δf/f), suggesting opposing activity patterns.
(b) Top: K-means clustering (k=4) over all cH and LH voxels reveals diverse clusters of activity. Number of voxels within each cluster is indicated next to the mean Δf/f trace. **Bottom:** Raster plots of clustered neurons sorted from the least active (blue) to most active (red) cluster.
(c) Calcium dynamics (integrated fluorescence and spike frequency) for each cluster over time reveal diverse activity patterns (5 min bins).
(d) Left: Average intensity projection images showing imaged regions. Cell bodies are outlined in white; for the LH they tend to correspond to the edges, whereas neuropil are more concentrated in the center. The cH comprises mainly cell bodies. **Right:** Positions of voxels corresponding to each cluster. Fish 2 is imaged at more ventral planes than fish 1.

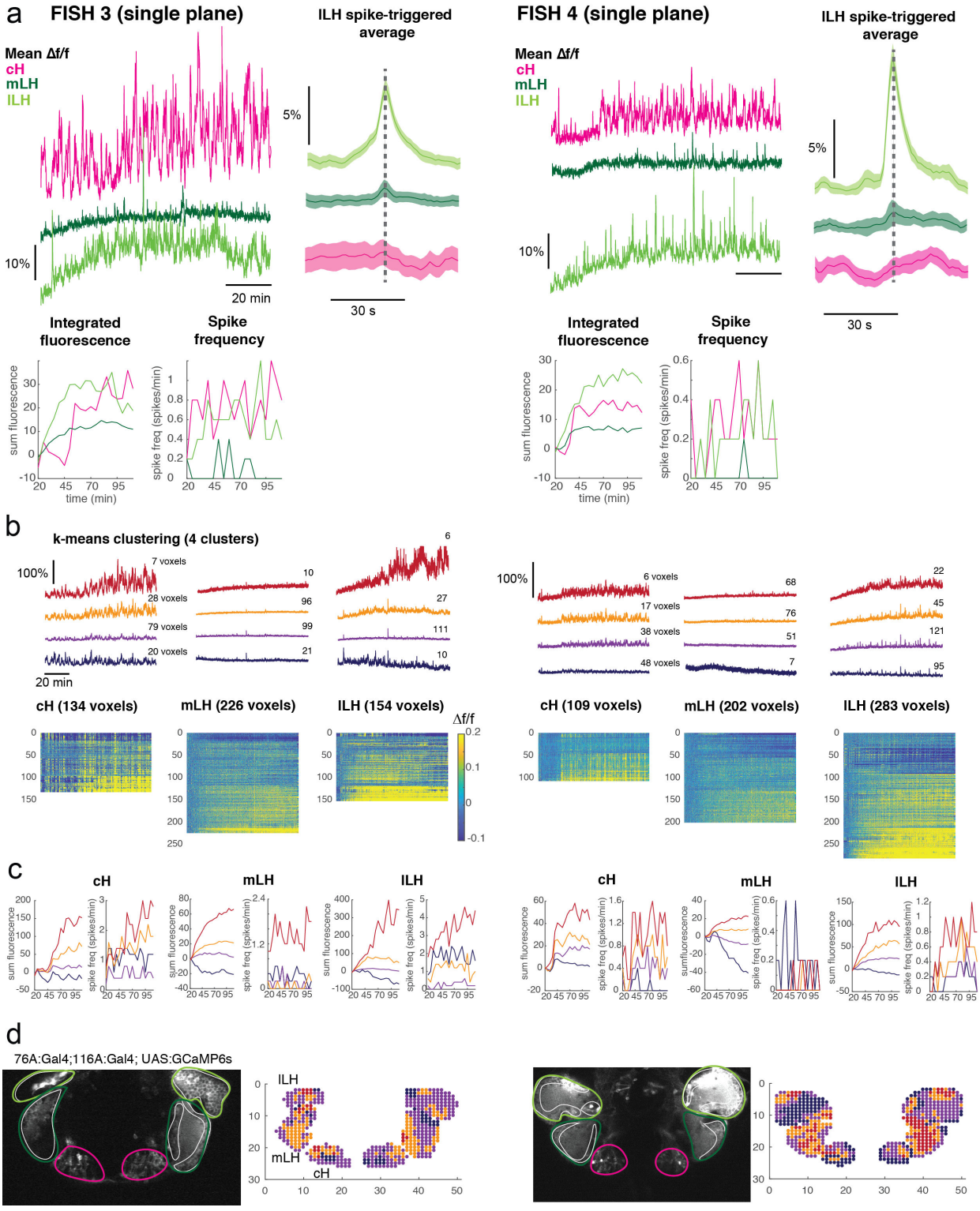

Figure 2 - Figure Supplement 5: Calcium imaging of cH and LH over food-deprivation reveal complex dynamics (single plane)

(a) Two fish (left and right) are shown. **Top left:** Mean Δf/f across the entire cH, mLH and lLH; **Bottom left:** calcium dynamics (integrated (sum) fluorescence and calcium spike frequency, 5 min bins) over the

course of a 2 hr long imaging session. Fish were imaged ~20 min after embedding, thus initial food-deprivation time is 20 min. **Right:** Spike-triggered averages based on lLH calcium spikes reveal an accompanying reduction in cH calcium fluorescence (Δf/f). As only a single-plane was imaged, the inverse relationship between the cH and LH is not as prominent.
(b) Top: K-means clustering (k=4) over all cH and LH voxels reveals diverse clusters of activity. Number of voxels within each cluster is indicated next to the mean Δf/f trace. **Bottom:** Raster plots of clustered neurons sorted from the least active (blue) to most active (red) cluster.
(c) Calcium dynamics (integrated fluorescence and spike frequency) for each cluster over time reveal diverse activity patterns (5 min bins).
(d) Left: Average intensity projection images showing imaged regions. Cell bodies are outlined in white; for the LH they tend to correspond to the edges, whereas neuropil are more concentrated in the center. The cH comprises mainly cell bodies. **Right:** Positions of voxels corresponding to each cluster. Since these fish were not embedded completely symmetrically, the left and right sides of the hypothalamus are at slightly different dorsal-ventral positions (right sides slightly more dorsal than left sides). Fish 3 is imaged at a more ventral plane than fish 4.

The caudal and lateral hypothalamus respond to food sensory cues and are anti-correlated over short timescales

We next examined the effects of food sensory cues on cH and LH activity dynamics by performing calcium imaging on tethered animals during the controlled presentation of food-related stimuli (Figure 3a). Consistent with the above results of pERK analysis of post-fixed brains, mLH and lLH neurons were strongly activated and cH neurons suppressed within seconds of paramecia addition to the water in the vicinity of a food-deprived fish (Figure 3b-c). Interestingly, neurons in all three hypothalamic loci responded to water flow alone (Figure 3b-c), with the cH and lLH responding more strongly than the mLH (Figure 3c, bottom panels). However, these responses were still significantly less than when paramecia were presented (Figure 3c, bottom panels). Thus, food (and other) sensory cues in the absence of hunting or food ingestion differentially modulate the activities of neurons in the caudal and lateral hypothalamic lobes.

We also observed that, across periods in which food cues were either present or absent, the activities of cH and LH neurons were remarkably anti-correlated; both spontaneous or food-induced fluctuations in one population were accompanied by a corresponding opposing change in the other (Figure 3b). This observation was supported by cross-correlation analysis between

cH, mLH and lLH voxels (Figure 3d-f), which revealed high correlation within the same hypothalamic region (red), and anti-correlation between cH and LH regions (blue) (Figure 3d-e). Further, lLH voxels showed more spatial heterogeneity than mLH voxels (Figure 3e), though a small cluster of cells at the most-anterior part of the lLH was found to be consistently anti-correlated with the cH (Figure 3e, Fish C and D, for example). When ranked according to their degrees of anti-correlation with voxels from other lobes, the cH and lLH appeared to show the greatest anti-correlation (Figure 3f). Overall, these results indicate that cH and LH neurons display generally anti-correlated activity over short timescales in addition to longer epochs reflecting states of hunger, voracious feeding and satiety.

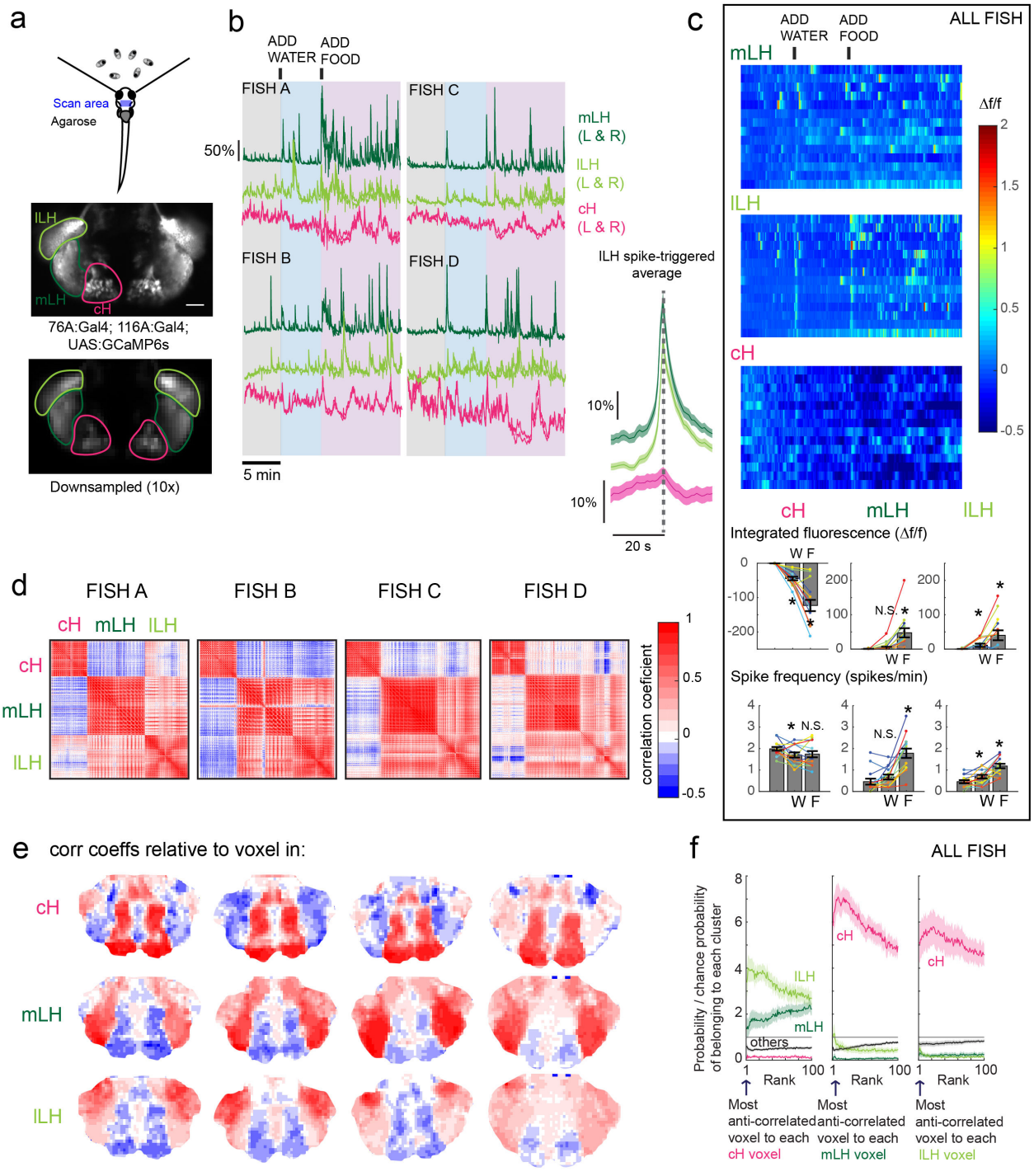

Figure 3: Anti-correlation on seconds timescale

(a) Top: Schematic showing the calcium imaging setup. Transgenic fish with GCaMP-labeled cH and LH neurons were paralyzed, tethered in agarose with their eyes and nostrils freed, and exposed to live paramecia. **Top image:** GCaMP expression in the cH and LH driven by two transgenic lines. **Bottom image:** Downsampled image stack used for analysis

(b) Left: Mean calcium activity from respective hypothalamic ROIs (shown in (i)) from 4 example fish after exposure to water (control) or paramecia. Left and right lobes are shown in same color and overlaid.

Paramecia presentation activates the LH and suppresses the cH, which show opposing activity on short timescales. **Right:** Average Δf/f triggered on lLH calcium spikes shows a mean corresponding reduction in cH activity (n = 159 lLH spikes extracted from mean Δf/f traces from 14 fish across the entire duration of the experiment)
(c) Top: Raster plots showing mean calcium activity from the mLH, lLH and cH of 14 fish before and after presentation of water and food cues. **Bottom:** Quantification of integrated (sum) Δf/f values and spike frequency (spikes/min) per fish across experimental epochs (300s baseline, 300s after water (W) delivery or 600 s after food delivery (F). Each colored line represents an individual fish. Water delivery was sufficient to significantly modulate both the cH ($p = 6.1 \times 10^{-5}$ (integrated fluorescence)/0.0497(spike freq.) and the lLH (p=0.029/0.026) but not the mLH (p = 0.48/0.055). Note though from **(b)** that the mLH does transiently respond to water delivery. Food delivery significantly increased mLH integrated fluorescence ($p=1.2 \times 10^{-4}$) and spike frequency ($p = 1.2 \times 10^{-4}$) relative to water delivery. Food delivery also significantly increased lLH integrated fluorescence (p =0.045) and spike frequency (0.0016) relative to water delivery. Food delivery significantly reduced cH integrated fluorescence further relative to water delivery ($p = 3.1 \times 10^{-4}$), but not spike frequency (p = 0.52). W = water, F = food. One-tail Wilcoxon Sign Rank Test.
(d) Cross-correlogram of hypothalamic cell-sized voxels (cells and/or neuropil from downsampled image stacks, see Figure 2a) from 4 example fish. cH and LH voxels were mostly anti-correlated, whereas voxels within each cluster had correlated activity.
(e) Correlation coefficients of other hypothalamic voxels relative to a voxel with the cH, mLH or lLH.
(f) Summary of data from 14 fish, showing the probability of the n^{th} most anti-correlated voxel belonging to each of the other clusters.

The activities of cH and LH neurons are differentially modulated by food sensory cues and ingestion

We next asked whether food sensory cues might have differential and independent effects from the consummatory cues elicited by the biting and swallowing of prey. Specifically, we tested the hypothesis that such ingestion cues might be necessary for the more sustained reciprocal changes in LH and cH activities that accompany voracious feeding. Since consummatory activity cannot be assessed in head-fixed animals, pERK analysis of activity was performed on post-fixed animals after free-swimming hunting and feeding behaviors. To distinguish between sensory and consummatory activities, we compared the neural activity of food-deprived fish upon exposure to either paramecia or artemia. Artemia are live prey commonly used to feed adult zebrafish, and are actively hunted by fish at all stages (Figure 4a, Video 2). They are however too large to be swallowed and consumed by larvae. Thus, the comparison between these two types of prey dissociates neural activity associated with prey detection and hunting from the neural consequences of food ingestion.

We found that with exposure to artemia it was not possible to detect a change in cH activity, but as observed above with live calcium imaging, exposure to this food cue in the absence of ingestion induced a small increase in lLH neural activity and a larger increase in mLH activity (Figure 4a-b). The artemia-induced hypothalamic activity was, however, less than that observed with consumable prey (Fig 4a-b). These observations suggest that the mLH responds primarily to sensory cues and/or induced hunting behavior whereas the induction of lLH activity largely depends on consumption. These data are furthermore consistent with the strong anti-correlation of cH with lLH activity (compared to mLH activity, Fig 3f), since both respond more strongly to food consumption rather than sensory cues. Thus, in addition to comprising distinct cell types (Figure 1- Figure Supplement 2), the lLH and mLH are also selective for different food cues, raising the possibility that they could be further specialized for distinct behavioral functions (Figure 4c, also see Discussion).

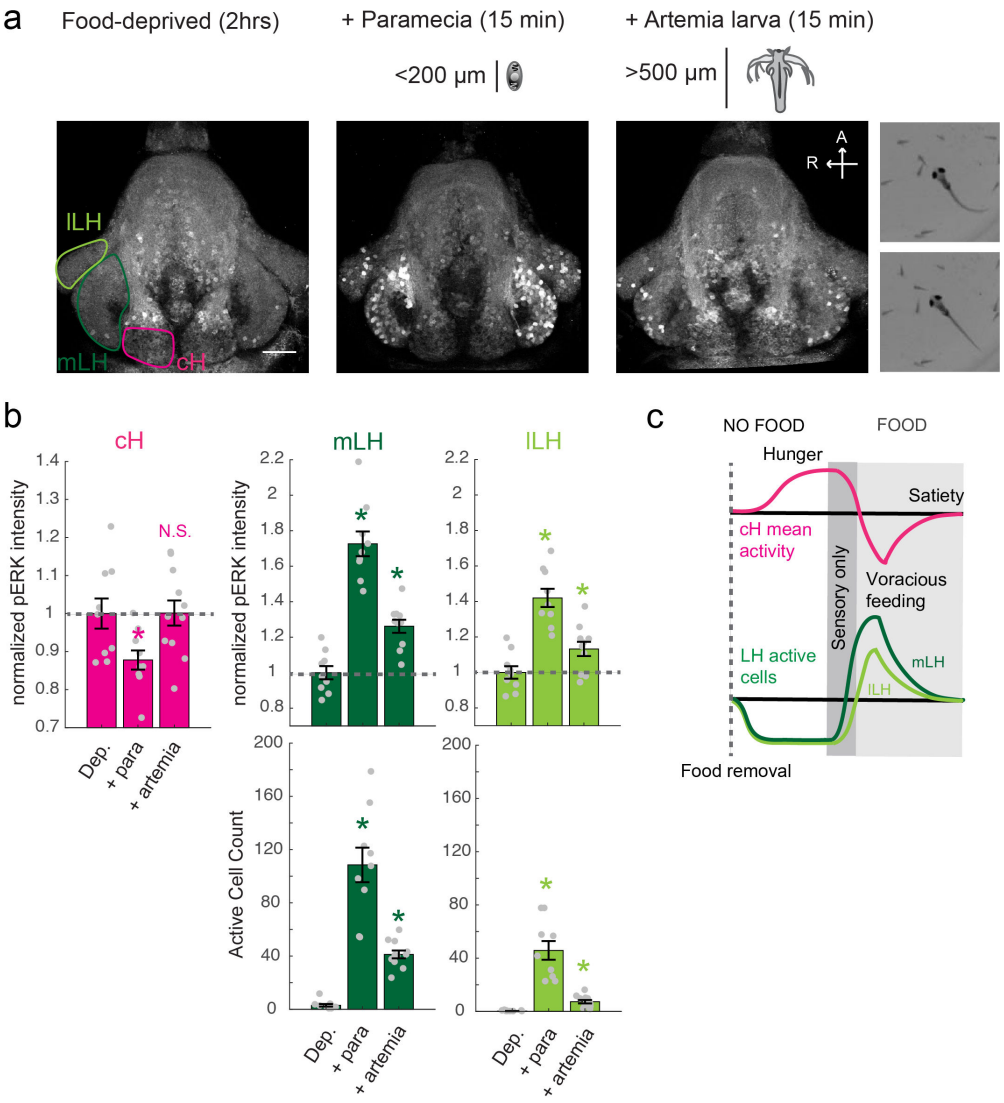

Figure 4: Sensory cues and food consumption differentially regulates cH and LH domains

(a) Representative images of pERK activity induced by paramecia vs artemia larvae. Hatched artemia are sensed and actively hunted by 7-8 dpf larval zebrafish, but too large to consume, allowing for the dissociation of sensory cues/hunting behavior and food consumption. Scale bar = 50 µm. Rightmost panel: Larval zebrafish attempt to hunt live artemia, performing J-bends and pursuits with eyes converged (Bianco et al., 2011). Also see Video 2.

(b) cH activity (normalized pERK intensity) is significantly reduced by paramecia but not by artemia ($p = 0.016$ (paramecia), 0.648 (artemia)). In contrast, the LH can be activated by artemia alone, though more strongly in the presence of paramecia. The lLH is more weakly activated than the mLH by artemia. Both normalized pERK intensity (mLH: $p = 2.06 \times 10^{-5}$ (paramecia), $p = 4.87 \times 10^{-4}$ (artemia); lLH: $p = 2.06 \times 10^{-5}$ (paramecia), $p = 0.033$ (artemia)), and active cell count (mLH: $p = 1.08 \times 10^{-5}$ (paramecia), $p = 6.02 \times 10^{-5}$ (artemia); lLH: $p = 1.08 \times 10^{-5}$ (paramecia), $p = 5.04 \times 10^{-5}$ (artemia)) are shown, with n = 8/9/11 fish, One-tail Wilcoxon Rank Sum Test).

(c) Revised schematic showing differential activation of cH and LH domains in response to food sensory vs consummatory cues.

Optogenetic cH activation suppresses lLH neural activity

The anti-correlated activity of the caudal and lateral hypothalamus suggests they might participate in mutual inhibition. We hypothesized that, during food deprivation, rising cH activity (along with the absence of food cues) suppresses LH activity, whereas the arrival of food cues and initial consumption that induces strong LH activity reciprocally shuts down cH activity. The reduction in cH activity, in turn, would permit higher LH activity, which may underlie voracious feeding behavior. Conversely, increased cH activity would reduce LH activity and return it to satiety levels.

In order to test our model that activation of cH neurons is sufficient to suppress LH activity, we expressed a red-shifted Channelrhodopsin (*Tg(UAS:ReaChR-RFP)*) in cH neurons (Dunn et al., 2016; Lin et al., 2013) and visualized LH neuronal activity via calcium imaging using *Tg(HuC:GCaMP6s)*. Since expression of ReaChR by the *Tg(116A:Gal4)* driver line was weak, we used a different Gal4 line, *Tg(y333:Gal4),* that labels a smaller fraction of serotonergic neurons in the cH (57.4±2.1%), but drives robust ReaChR expression (Figure 5 – Figure Supplement 1). In addition, the *Tg(UAS:GGaMP6s)* transgene was expressed in some animals, allowing us to monitor optogenetically-induced cH activity. In these animals, ReaChR stimulation (10-15 seconds, 633 nm laser illumination) and subsequent calcium imaging confirmed strong activation of the cH. Significantly, optogenetic stimulation of the cH reduced spontaneous lLH activity (Figure 5b, d), but did not alter mLH activity. Hence it appears that cH activity is sufficient to inhibit lLH but not mLH activity. This distinction may allow mLH neurons to remain sensitive and responsive to food cues under food-deprivation conditions, while cH activity is elevated.

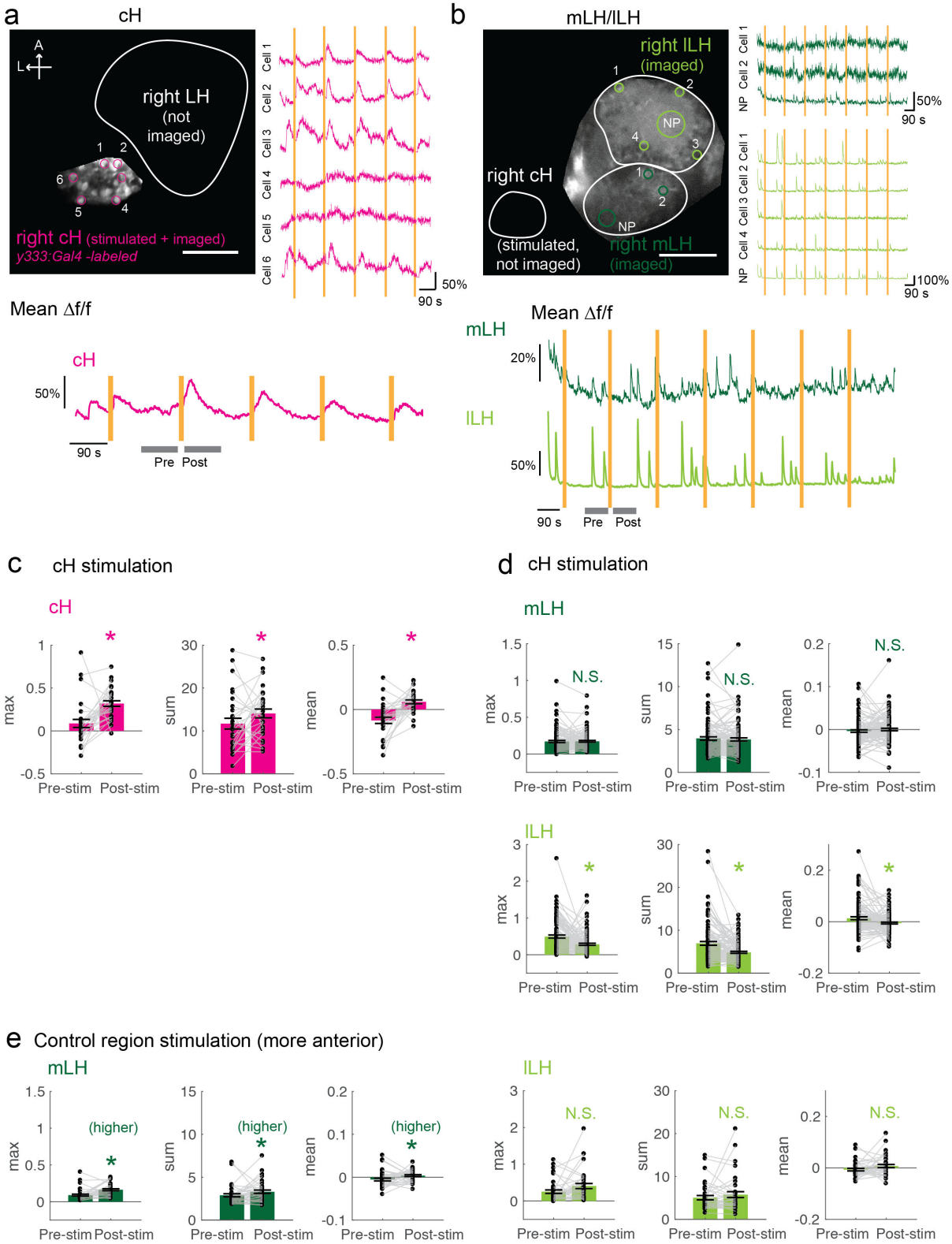

Figure 5 with 1 supplement: Optogenetic cH stimulation is sufficient to reduce lLH activity

(a) Stimulation of cH neurons in *Tg(y333:Gal4;UAS:ReaChR-RFP;UAS:GCaMP6s)* fish with a 633 nm laser induces sustained activation in a fraction of cells. Image shows confocal imaging and stimulation

area, numbers depict individual cells whose activities (Δf/f) are shown on the right. Scale bar = 50 μm. Bottom: Mean Δf/f across the entire ROI over time. Orange bars = 10 second stimulation period (no imaging occurs during that period). Gray bars indicate pre- and post-stimulation period over which activity will be averaged.

(b) Stimulation of cH neurons in a different fish expressing *Tg(y333:Gal4;UAS:ReaChR-RFP; HuC:GCaMP6s)* reduces spontaneous activity in lLH neurons. The cH was not imaged simultaneously as ReaChR can be activated by higher-intensity 488 nm light (see methods). Image shows confocal imaging and stimulation area, numbers depict individual cells or neuropil (NP) whose activities (Δf/f) are shown on the right. It was not always possible to resolve individual LH cells in other imaged fish. Scale bar = 50 μm. Bottom: Mean Δf/f across mLH and lLH ROIs over time.

(c-e) Comparison of mean and maximum Δf/f for a 90 s window before and after ReaChR stimulation. Each data point represents a single stimulation.

(c) cH activity increases after ReaChR stimulation. N = 29 stimulations across 8 fish, p = 0.0002(max)/0.036(sum)/9.2×10^{-5}(mean), One-tail Wilcoxon sign rank test.

(d) mLH activity does not change after ReaChR stimulation (p = 0.74 (max)/0.85 (sum)/0.13 (mean)), whereas lLH activity is significantly suppressed after ReaChR stimulation (p = 0.0003(max)/1.8×10^{-6} (sum)/0.049(mean)). N = 108 stimulations across 9 fish. Two-tail Wilcoxon sign rank test.

(e) Stimulation of a control area (i.e. more anterior to cH and unlabeled by ReaChR) tends to increase activity in the mLH (p = 0.0003(max)/0.039(sum)/0.039(mean) and does not change lLH activity (p = 0.099(max)/0.65(sum)/0.096(mean). N = 37 stimulations from 5 fish. Two-tail Wilcoxon sign rank test.

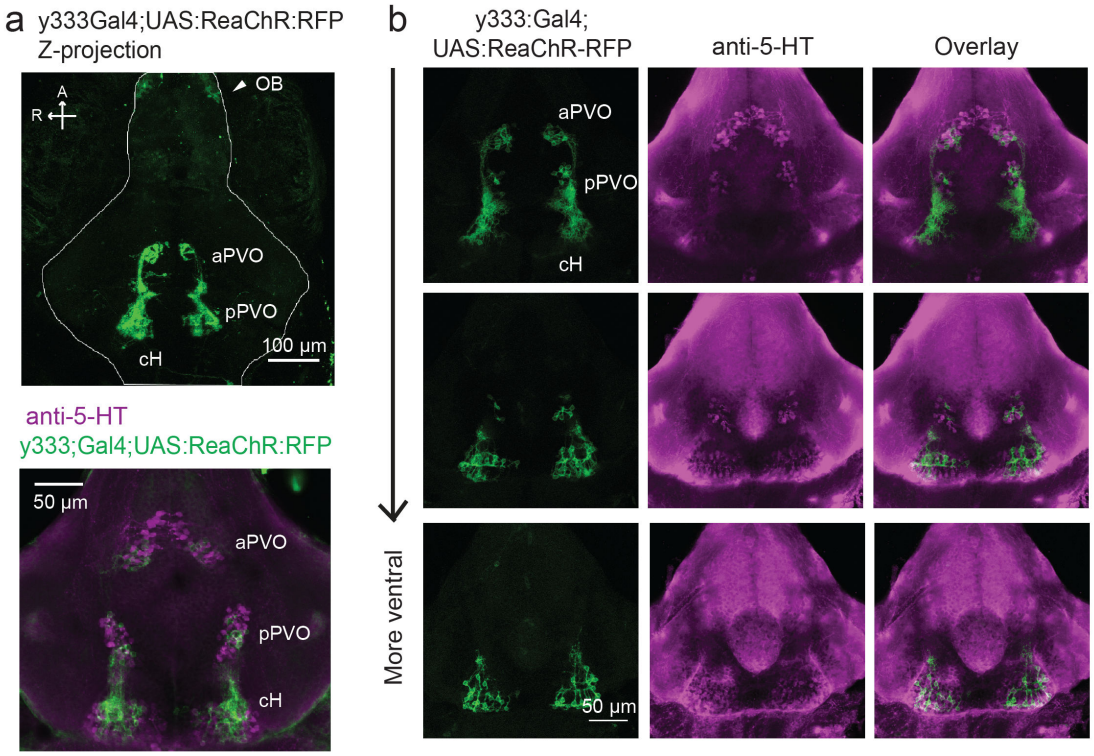

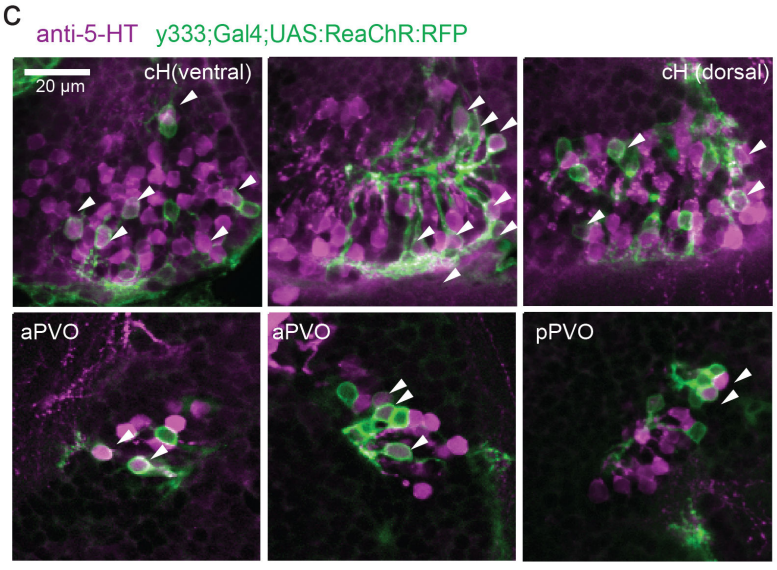

d

y333:Gal4;UAS:ReaChR-RFP

aPVO

Fish	y333+	y333+/5-HT+	% Overlap
1	12	7	58.3%
2	35	20	57.1%
3	19	10	52.6%
4	16	8	50.0%
MEAN	**20.5**	**11.3**	**54.5%**
ERR	**5.04**	**2.98**	**1.95%**

pPVO

Fish	y333+	y333+/5-HT+	% Overlap
1	13	6	46.2%
2	29	15	51.7%
3	20	9	45.0%
4	19	9	47.4%
MEAN	**20.3**	**9.8**	**47.6%**
ERR	**3.30**	**1.89**	**1.47%**

cH

Fish	y333+	y333+/5-HT+	% Overlap
1	44	26	59.1%
2	87	54	62.1%
3	50	28	56.0%
4	59	31	52.5%
MEAN	**60.0**	**34.8**	**57.4%**
ERR	**9.51**	**6.50**	**2.05%**

Figure 5- Figure Supplement 1: Characterization of the y333:Gal4 line

(a) We used an alternative cH-labeling Gal4 line, *Tg(y333:Gal4)* (Marquat et al (2015), to drive *Tg(UAS:ReaChR-RFP)* expression, as we were unable to detect any ReaChR expression using *Tg(116A:Gal4)*. **Top:** Whole mount stack of a *Tg(y333:Gal4;UAS:ReaChR-RFP)* (green) shows relatively specific expression in the caudal hypothalamus, as well as some labeling in the olfactory bulb (white arrow) and other scattered cells. Scale bar = 100 µm. Bottom: Z-projection image of a dissected fish

brain mounted ventral side up, with anti-5-HT staining shown in magenta. Scale bar = 50 μm. **(b)** Overlap of *Tg(y333:Gal4;UAS:ReaChR-RFP)* (green) with anti-5-HT immunostaining (magenta) is seen in all layers of the caudal hypothalamus, and also the paraventricular organ (PVO), though the degree of overlap is less for the PVO. Each row shows a different Z-plane, moving from more dorsal to more ventral. Dissected fish brains mounted ventral side up. Scale bar = 50 μm. **(c)** Higher magnification image showing moderate overlap of *Tg(y333:Gal4;UAS:ReaChR-RFP)* with anti-5-HT staining in the cH and PVO. Arrows indicate cells with overlapping RFP and 5-HT expression. Scale bar = 20 μm. **(d)** Quantification of overlap between 5-HT and *Tg(y333Gal4;UAS:ReaChR-RFP)* expression in the cH and PVO.

Functional dissection of cH serotonergic neurons in feeding behavior

The opposing patterns of cH and LH activities suggest that they might have opposing roles in the control of hunting and feeding behavior. Given that the cH is composed of neuromodulatory populations, including serotonergic neurons, and is sufficient to suppress lLH neural activity, we reasoned that these cH neurons might act as a homeostatic regulator of satiation state-dependent food intake. In particular, we postulated that: 1) higher cH activation prior to feeding would encode a state of hunger and enhance the animal's sensitivity to subsequent food cues, and 2) higher cH activation during feeding would oppose lLH activity to suppress food intake. To test this hypothesis, we combined ReaChR activation of cH neurons with quantitative measurements of food intake, again using the y333:Gal4 transgenic line. When satiated (continuously fed) fish were exposed to whole field orange (630 nm) light for 10 minutes prior to food presentation, fish in which ReaChR was expressed in the cH consumed significantly more paramecia than fish that lacked *Tg(y333:Gal4;UAS:ReaChR-RFP)* expression (Figure 6a). This effect was not observed for food-deprived fish, perhaps because they already display high cH activity and a high rate of feeding (Figure 6a). These observations are consistent with the interpretation that optogenetic cH activation simulated a food-deprived state in satiated fish and thus enhanced their subsequent feeding.

In contrast to the outcome of optogenetic activation prior to feeding, the induction of cH activity during food presentation reduced feeding, especially in food-deprived fish (Figure 6b). These observations indicate that optogenetic cH activation can reduce feeding, particularly in

588 animals in which cH activity is low (Figure 6b, Figure 6 - Figure Supplement 1). Accordingly, we
589 propose that optogenetic stimulation of cH activity inhibits lLH activity and thereby causes the
590 feeding rate to decrease.

591 Finally, we asked what would happen if we directly reduced net cH activity via partial
592 ablation of the serotonergic population. We hypothesized that this would induce a constitutively
593 low cH activity, which should enhance food intake regardless of satiation state. Thus, we
594 performed chemical-genetic ablations of serotonergic cH neurons labeled by *Tg(116A:Gal4;*
595 *UAS:nfsb-Cherry)* (Curado et al., 2008), and compared the feeding rates of ablated animals to
596 that of sibling controls (Figure 6c). Food ingestion was examined in animals in which cH
597 neurons were partially ablated (see Figure 6 - Figure Supplement 2 and legend for details) and
598 compared to that of their non-ablated siblings, who lacked *Tg(116A:Gal4;UAS:nfsb-Cherry)*
599 expression (Figure 6c). We observed a significantly increased food intake for ablated fish in
600 both food-deprived and fed conditions, indicating that regardless of prior activity patterns, low
601 cH activity in the presence of food is what ultimately controls food consumption.

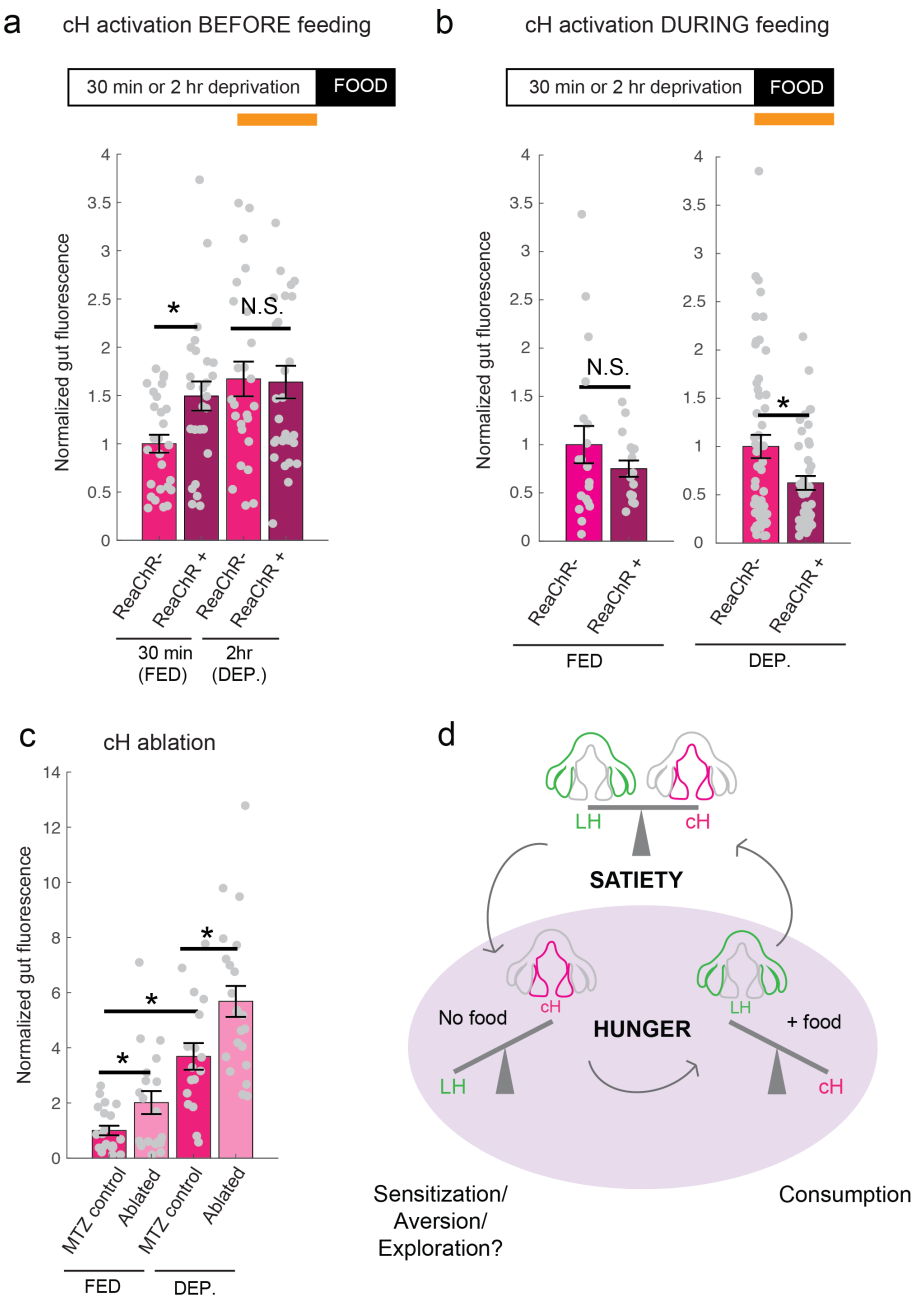

Figure 6 with 3 supplements: Role of the cH in behavioral control

(a) Optogenetic activation (orange bar in schematic) of the cH 10 min prior to feeding increases food intake in fed fish (i.e. 30 min food-deprived), but not food-deprived (2hr food-deprived) fish, during subsequent food presentation. Fed: n = 27/26 (ReaChR-/ReaChR+), p = 0.005. Food-deprived: n = 25/29 (ReaChR-/ReaChR+), p = 0.36, One-tail Wilcoxon Rank Sum Test. Since ReaChR expression via 116A:Gal4 was negligible, we used another Gal4 (*Tg(y333:Gal4)*) line that is also specific to the cH when ReaChR is expressed. Fed and food-deprived fish were assayed simultaneously, thus all results was normalized to fed controls. ReaChR- controls do not have visible *Tg(y333:Gal4;UAS:ReaChR-RFP)* expression, and thus are a mixture of siblings expressing *Tg(y333:Gal4) only*, *Tg(UAS:ReaChR-RFP)* or neither of these transgenes, each with ⅓ probability.

(b) Left: Optogenetic activation of the cH (orange bar in schematic) during feeding in fed fish does not

significantly reduce food intake. n = 19/16 (ReaChR-/ReaChR+), p = 0.44 (N.S.), Right**:** Optogenetic activation of the cH during feeding in food-deprived fish reduces food intake. n = 53/44 (ReaChR-/ReaChR+), p = 0.042. Since fed and food-deprived fish were assayed in different experiments, gut fluorescence normalized to their respective controls, One-tail Wilcoxon Rank Sum Test.
(c) Nitroreductase-mediated ablation of the cH in (*Tg(116A:Gal4;UAS-nfsb:mCherry)* or negative fish treated with metronidazole from 5-7 dpf significantly enhances food intake in 8 dpf fish. p = 0.004/0.04/1.4x10^{-5} (fed control vs ablated, dep. control vs ablated, fed vs dep.). Controls do not have visible *Tg(116A:Gal4;UAS:nfsb-mcherry)* expression, and thus are a mixture of siblings expressing *Tg(116A:Gal4) only*, *Tg(UAS:nfsb-mcherry)* or neither of these transgenes, each with ⅓ probability.
(d) Schematic summarizing our results. We propose distinct roles of the cH during hunger, depending on the presence or absence of food. See Supplementary File 1 – Conceptual Circuit Model for elaboration.

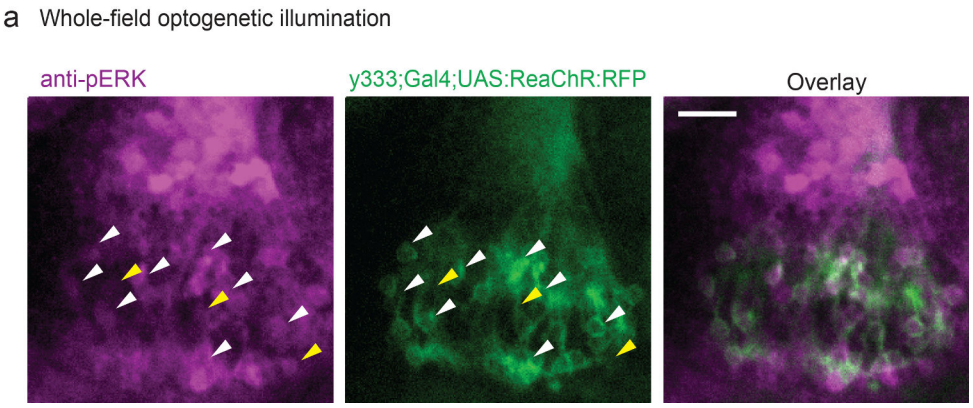

Figure 6 – Figure Supplement 1: ReaChR activation by whole-field optogenetic illumination
(a) *Tg(y333:Gal4;UAS:ReaChR-RFP)* stimulation during feeding is sufficient to induce pERK activity in many transgene-positive neurons. White arrows point to a few examples where *Tg(y333:Gal4;ReaChR-RFP)* expression corresponds to more intense pERK staining. Yellow arrows point to examples in which ReaChR expression is visibly absent, which appears to correspond to weaker pERK staining. ReaChR expression looks hazy as it was photobleached by the end of the 10 min stimulation period. Scale bar = 20 μm.

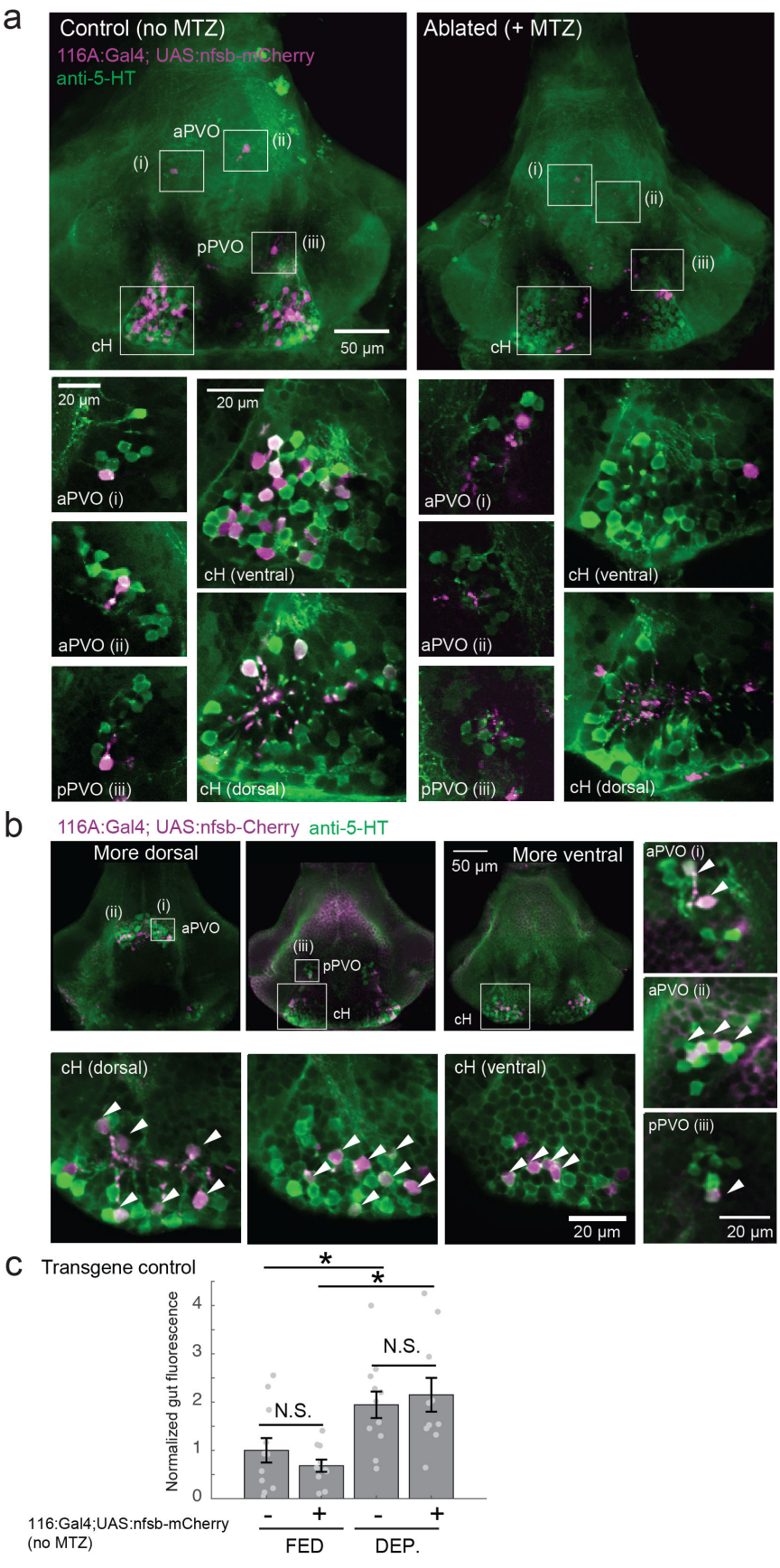

Figure 6 - Figure Supplement 2: Nitroreductase-mediated ablation of cH neurons

(a) Effective ablation of *Tg(116A:Gal4;UAS:nfsb-mCherry)*-labeled neurons using MTZ. Note that due to sparser expression, ablation of the cH/PVO populations are likely to be partial (<50%). Representative projection images are shown of non-ablated (left) and ablated fish brains (right). Scale bar = 50 μm. Insets roughly labeled by white boxes show higher-magnification single-plane images of cH, aPVO and pPVO labeling by this transgene, and overlap with 5-HT expression. Overall, since the labeling of cH neurons with nitroreductase-mCherry is relatively weak (~ 6-8 cells in the aPVO, ~2-4 cells in pPVO, and ~30-40 cells in the cH), our ablations are only partial and may include a few PVO neurons. Scale bar = 20 μm.

(b) Similar to Tg (116A:Gal4;UAS:GFP, there is high overlap of *Tg(116A:Gal4;UAS:nfsb-mCherry)* with anti-5-HT immunostaining. Scale bar = 50 μm. Insets roughly labeled by white boxes show higher-magnification single-plane images of cH, aPVO and pPVO labeling by this transgene, and overlap with 5-HT expression. Scale bar = 20 μm.

(c) The *Tg(116A:Gal4;UAS:nfsb-mCherry)* transgene does not affect feeding in the absence of MTZ, relative to non-expressing siblings. Fed: p = 0.64, n = 11(negative)/10(positive); Dep.: p = 0.91, n = 11(negative)/10(positive), Fed vs Dep.: p = 0.035 (negative)/7.7×10^{-4}(positive).

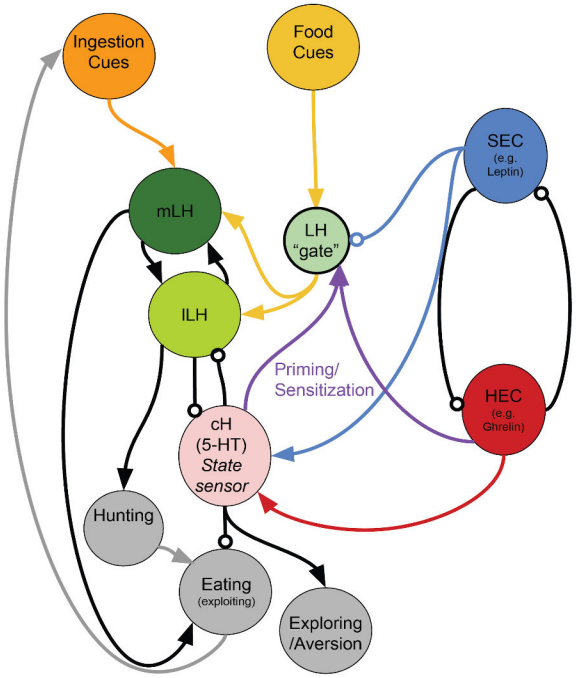

Figure 6 - Figure Supplement 3: A conceptual circuit model of the cH/LH hypothalamic network

HEC = Hunger Encoding Circuit, SEC = Satiety Encoding Circuit, which should have anti-correlated activities and report the animal's energy/caloric status. The cH represents both hunger and satiety state and sensitizes (or primes) the LH during hunger. It may drive other behaviors such as exploration or aversive behavior, but also suppresses feeding. Other HEC components may also be involved in LH sensitization. We propose mutual inhibition between the cH and LH, though we have only demonstrated unidirectional inhibition (cH on lLH) thus far. The mLH, normally responsive to food cues, may promote hunting, though not necessarily coupled with ingestion, whereas the lLH, which is more responsive to ingestive cues, should enhance further ingestion (i.e. eating). The LH "gate" is a conceptual representation of how its sensitivity to food cues could be modulated by other signals (i.e. reduced by the SEC and enhanced by cH-mediated sensitization). It does not necessarily represent a physical neuronal population. More elaboration can be found in Supplementary File 1 – Conceptual Circuit Model.

DISCUSSION

Decades-old studies on appetite regulation in mammals have suggested modular hypothalamic units that work to suppress or enhance food intake respectively. Here, we show that the larval zebrafish hypothalamic network can similarly be functionally divided into its medial and lateral units. These units show anti-correlated activity patterns during various states that relate to ingestive behavior, such as hunger and voracious eating, and energy homeostasis is reflected by a restoration of balance between these areas (Figure 6d). Furthermore, we show that within these broad neural response classes lies a diversity of neurons that encode specific stimuli and perform distinct functions depending on the timing of activation.

Mutually opposing hypothalamic networks control zebrafish appetite

We show that the medial hypothalamic zone, especially the caudal hypothalamus (cH) in the zebrafish, is strongly activated by food-deprivation, and strongly inhibited during voracious feeding, and that this happens on a timescale of seconds to minutes. Here, we focused mainly on the serotonergic cH neurons, although many medially localized neurons may show similar activity patterns. In contrast, the lateral hypothalamus (LH), which contains GABAergic and glutamatergic neurons, is inhibited in the absence of food and most strongly activated during voracious eating. Interestingly, satiated fish exhibit intermediate activity levels in both hypothalamic regions. Thus, hunger in the presence and absence of food is represented by two distinct states of activity in opposing brain regions, with restoration of energy homeostasis paralleled by a balance of the network.

While generally anti-correlated, the cH and LH also appear to be differentially modulated by both internal (i.e. hunger cues) and external factors (i.e. food). In the absence of food, LH cellular activity decreases rapidly, suggesting a requirement of food/other external cues to drive LH activity, though some modest rate of spontaneous activity is still observed. On the other hand, the slower timescales of cH activation appears to reflect the animal's rising caloric deficit.

Notably, many of the cH neurons are cerebrospinal fluid-contacting and thus have access to circulatory information (Lillesaar, 2011; Pérez et al., 2013).

Further, despite clear reductions in pERK cellular activity, calcium imaging has revealed more complex dynamics of the LH over food-deprivation. These changes could be induced by the generally aversive and potentially unnatural internal state of a head-fixed preparation, or, more intriguingly, could reflect an increased sensitivity of LH neurons over the course of hunger. These hypotheses can potentially be distinguished in future work by performing calcium imaging of hunting and feeding behavior in a free-swimming setting (Kim et al., 2017).

Once food becomes available (but when caloric deficit is still high), a state change occurs, and LH activity is strongly enhanced whereas cH activity is strongly suppressed. Importantly, the degree of cH suppression and LH activation are correlated with the extent of prior food-deprivation, suggesting a role for these nuclei in regulating food intake based on caloric needs. This striking anti-correlation between the cH and LH suggests a mutual inhibition, and that an acute reduction in cH activity is what allows for the enhanced LH release.

We have partially confirmed the hypothesis of such mutual inhibition using optogenetic stimulation of the cH and simultaneous calcium imaging of the LH. We show that activation of the cH is sufficient to drive down lLH, but not mLH activity. Consistent with these results, the cH appears to be more strongly anti-correlated with the lLH than the mLH.

However, the mechanisms by which cH might influence LH activity, and vice versa, are still unknown. It is possible that the cH may act via inhibitory GABAergic neurons, and/or exert their effects through direct secretion of monoamines into the ventricles or perineuronal space. The effect of cH optogenetic activation on lLH activity appears to persist for minutes, allowing for the possibility of direct neuromodulatory action. At the same time, there appears to be a fast (seconds) anti-correlation between cH and LH calcium activity, suggesting faster inhibitory connections. The LH, which was previously characterized in Muto et. al (2017), similarly does not appear to send direct projections to the cH, but could potentially interact via intermediary

720 neurons in the medial/periventricular regions of the hypothalamus.

721

722 *Food cues differentially regulate cH and LH domains*

723 Ingestive behavior has been proposed to comprise a number of temporal stages: 1) the
724 initiation phase, triggered by energy deficit, in which the animal begins to forage; 2) the
725 procurement phases, triggered by the presence of food sensory cues, in which the animal seeks
726 and pursues food; and 3) the consummatory phase, which involves a more stereotyped motor
727 program (Berthoud, 2002; Watts, 2000). An animal's energy status is sensed internally and may
728 influence the initiation, procurement and consummatory stages of ingestive behavior. Thus, a
729 hungry animal will be more alert to food cues, seek food more persistently and also eat it more
730 voraciously.

731 In mammals, LH neurons are responsive to both external food sensory cues and
732 consummatory cues (Jennings et al., 2015). Here, we show that the LH lobes in zebrafish also
733 respond differentially to food cues in an anatomically segregated manner. In this "sensory"
734 stage, the mLH is already activated, which may reflect an enhanced sensitivity to food cues
735 during hunger. However, mLH activation during this sensory stage is not as strong as post-food
736 consumption. In contrast, the lLH is only weakly activated by food cues, and cH activity
737 transiently falls but remains overall high. Thus, taken together with our optogenetic and calcium
738 imaging data, the mutually inhibitory circuit model is most consistent between the cH and lLH
739 (though the mLH is still generally anti-correlation with cH activity, especially in the presence of
740 food).

741 Since lLH and cH activity are modulated within minutes of food consumption they are
742 unlikely to reflect satiety signals, and rather might play a role in further driving voracious food
743 consumption, at least until the activity of both populations returns to baseline. In contrast, the
744 mLH may pay a role in enhancing the sensitivity of the animal to external food sensory cues,
745 even prior to initial food consumption.

It is unclear which consummatory cues modulate lLH and cH activity. Based on live imaging results from Muto et al (2017), the greatest enhancement of LH activity was observed almost immediately (milliseconds to seconds) after paramecia consumption. Thus, the cue is likely a fast pregastric signal (taste/tactile/swallowing), rather than postgastric absorption or hormone secretion.

Functional roles of the cH and LH in and beyond appetite control

Finally, we test the hypothesis that the cH and LH form mutually antagonistic functional units that dominate different phases of hunger and drive appropriate behavioral responses during each phase. In particular, we show that the activation state of the cH is a crucial regulator of satiation-state dependent food intake. Artificial cH activation in satiated fish *prior* to feeding is sufficient to drive subsequent voracious feeding. Based on observed cH dynamics, we propose that the degree on cH inhibition during voracious feeding is proportional to the degree of cH activation prior to feeding. This could be mediated by the release of serotonin/other neuromodulators over the course of food-deprivation, which may be capable of sensitizing the LH even in the absence of food cues. An intriguing, though untested hypothesis is that the rise in LH calcium fluorescence during food-deprivation, that tends to parallel that of cH activity, may reflect such sensitization. In this way, zebrafish are able to retain a “memory” of their hunger state, which is released once food is presented, and up-regulate their feeding behavior accordingly. This motif might help ensure that the animal eventually returns to a stable equilibrium, that is, satiety.

We furthermore show that the acute effect of cH activation *during* feeding is suppression of food intake, whereas cH ablation enhances food intake, which is again consistent with mammalian studies of medial hypothalamic areas. At first glance, the observation that the cH acutely suppresses food intake is inconsistent with the idea that it is most active during hunger. However, our optogenetic experiments show that the context of cH activation needs to be taken

772 into consideration, and can have opposing results on feeding. In the presence of food, activation
773 of the cH may simply drive down LH activity, hence reducing food intake. This is assuming that
774 any sensitizing effect of cH activation is weaker than the acute inhibitory effect of cH activation
775 on lLH activity, a conclusion that appears to be validated by our behavioral results.

776 The seemingly paradoxical roles of the cH during hunger may also make sense when
777 considering that, in the absence of food, consummatory behavior would in fact be
778 counterproductive. Thus, during food-deprivation, the cH may play complementary roles such as
779 the sensitization of the LH and/or other feeding-related circuits (as discussed above), or drive
780 alternative behavioral programs, like foraging or energy-conserving measures during this stage
781 of hunger (see Supplementary File 1 - Conceptual Circuit Model for a more in-depth discussion).
782 Given that cH neurons appear also to be activated by aversive stimuli (Randlett et al., 2015), it
783 may also more generally encode a negative valence state in the absence of food. Similar
784 features of hunger-related (i.e. AgRP) neurons have also been described in mammals (Betley et
785 al., 2015; Chen et al., 2015; Dietrich et al., 2015; Mandelblat-Cerf et al., 2015).

786 Although the cH does not have an exact mammalian homolog, its functions have been
787 proposed to be adopted by other modulatory populations, such as the serotonergic raphe
788 nucleus in mammals (Gaspar and Lillesaar, 2012; Lillesaar, 2011). While known to be a potent
789 appetite suppressant, serotonin is also released during food deprivation, and has been shown to
790 enhance food-seeking behavior (Elipot et al., 2013; Kantak et al., 1978; Pollock and Rowland,
791 1981; Voigt and Fink, 2015). Thus, our results showing opposing cH activity patterns during
792 hunger could reflect similarly complex roles of serotonin in zebrafish, potentially explaining
793 some of its paradoxical functions. The cH and PVO also express dopaminergic (intermingled
794 with 5-HT) and histaminergic neurons (in the surrounding cell-layer of the cH), which appear to
795 be densely interconnected (Kaslin and Panula, 2001). We note that our data, while confirming a
796 role of serotonergic neurons, does not rule out an involvement of these other neuromodulators
797 in appetite control.

798 Further, our results do not rule out the involvement of other circuits in appetite control; in
799 fact, they suggest that there are numerous players involved. For example, the PVO appears to
800 be modulated by food cues and food-deprivation, is anti-correlated with LH activity, and labeled
801 by our transgenic lines (albeit more sparsely), suggesting it may complement the role of the cH.
802 Our conclusions are also limited by available tools and methodologies -- since different
803 transgenic lines were utilized for stimulation and ablation, we cannot be certain that we are
804 manipulating the same population of neurons, though both share mutual overlap with
805 serotonergic cells. Also, due to the lack of complete transgene specificity, there is a possibility
806 that our manipulations may affect non-specific targets such as the olfactory bulb.
807 Similarly, while the strong LH activation after food-deprivation suggests that it might
808 promote voracious feeding, we were unable to assay the effect of LH activation in larval
809 zebrafish, due to broad and unspecific expression within the LH-labeling transgenic line.
810 However, Muto et al (2017) recently demonstrated that inhibition of the LH impairs prey capture
811 behavior, though they did not implicate the LH in the regulation of food intake based on hunger
812 state. Furthermore, electrical stimulation of the homologous region (lateral recess nuclei) in
813 adult cichlids and bluegills (Demski, 1973; Demski and Knigge, 1971) can elicit feeding
814 behavior, which is consistent with our hypothesis. Interestingly, while stimulating some of these
815 regions induced food intake, other induced behaviors, such as the “snapping of gravel”, were
816 reminiscent of food search or procurement. In mammals, electrical or optogenetic stimulation of
817 LH neurons triggers voracious eating, again consistent with our findings that the LH is highly
818 activated during the voracious eating phase in hungry fish (DELGADO and ANAND, 1953). In
819 particular, GABAergic neurons that do not co-express MCH or Orexin have been shown to be
820 responsive to food cues and are sufficient to stimulate food intake in mammals (Jennings et al.,
821 2015). Whether these GABAergic and glutamatergic neurons of the zebrafish LH co-express
822 other neuromodulators, as has been recently discovered in mammals (Mickelsen et al., 2019),
823 remains to be explored. Overall, these data suggest that the zebrafish LH may similarly play an

important role in driving food intake during hunger, despite some differences in peptidergic expression from mammalian LH. Certainly, since cues such as water flow and optogenetic stimulation light are sufficient to modulate cH and/or LH neurons, these hypothalamic loci are likely also involved in other sensorimotor behaviors beyond appetite regulation.

In conclusion, we have shown here how anatomically segregated hypothalamic networks might interact to control energy homeostasis. We argue that the medial-lateral logic of hypothalamic function may be conserved even in non-mammalian vertebrates, though their activity patterns may possibly be more complex than originally believed. Our data suggests diverse roles of neuromodulators such as serotonin in regulating behavioral responses during hunger, which may complement mammalian observations. Finally, we propose that investigating large-scale network dynamics may reveal an additional layer of insights into the principles underlying homeostatic behavior, which might be overlooked when studies are restricted to the observation and perturbation of a small subpopulation.

SUPPLEMENTARY FIGURE LEGENDS

Supplementary Table 1: Z-brain anatomical regions that are more activated in voraciously feeding (food-deprived + food) fish as compared to fed fish.

Supplementary Table 2: Z-brain anatomical regions that are more activated in fed fish as compared to voraciously feeding (food-deprived + food) fish.

Video 1: Z-stack (dorsal to ventral) of brain activity map shown in Figure 1b.

Video 2: Video of larval zebrafish hunting artemia larvae. Prey-capture behavior, such as J-bends and pursuits, but no capture swims, were observed in response to artemia larvae. Recording rate: 30 fps. Playback rate: Real time.

Supplementary File 1: Conceptual Circuit Model
A comprehensive overview of our circuit model and current understanding, including a circuit diagram, detailed elaboration and testable predictions.

MATERIALS AND METHODS

Key Resource Table

Reagent type (species) or resource	Designation	Source or reference	Identifiers	Additional information
genetic reagent *(danio rerio)*	*Tg(pGal4FF:116A)*	Characterized in this manuscript		Dr. Koichi Kawakami (NIG, Japan)
genetic reagent *(danio rerio)*	*Tg(pGal4FF:76A)*	PMID: 28425439		Dr. Koichi Kawakami (NIG, Japan)
genetic reagent *(danio rerio)*	*Tg(y333:Gal4)*	PMID: 26635538		Dr. Harold Burgess (NIH)
genetic reagent *(danio rerio)*	*Tg(HuC:GCaMP6s)*	PMID: 28892088		Dr. Florian Engert (Harvard)
genetic reagent *(danio rerio)*	*Tg(UAS:GCaMP6s)*	PMID: 28425439		Dr. Koichi Kawakami (NIG, Japan)
genetic reagent *(danio rerio)*	*Tg(UAS:GCaMPHS)*	PMID: 22046464		Dr. Koichi Kawakami (NIG, Japan)
genetic reagent *(danio rerio)*	*Tg(UAS:ReaChR-RFP)*	Characterized in this manuscript		Dr. Misha Ahrens (Janelia Research Campus)
genetic reagent *(danio rerio)*	*Tg(UAS-E1b:NTR-mCherry)*	PMID: 17335798		Available from ZIRC
genetic reagent *(danio rerio)*	*Tg(Vglut2a:dsRed)*	PMID: 19369545		
genetic reagent *(danio rerio)*	*Tg(Gad1b:loxP-dsRed-loxP-GFP)*	PMID: 23946442		
genetic reagent *(danio rerio)*	*Tg(Gad1b:GFP)*	PMID: 23946442		
genetic reagent *(danio rerio)*	*Tg(TH2:GCamP5)*	PMID: 26774784		Dr. Adam Douglass (University of Utah)

genetic reagent *(danio rerio)*	*Tg(ETvmat2:GFP)*	PMID:18164283		
genetic reagent *(danio rerio)*	*Tg(HCRT:RFP)*	PMID: 25725064		
antibody	Rabbit monoclonal anti-pERK	Cell Signaling	4370 RRID:AB_2315112	IHC (1:500)
antibody	mouse monoclonal anti-ERK	Cell Signaling	4696 RRID:AB_390780	IHC (1:500)
antibody	rabbit polyclonal anti-5-HT	Sigma-Aldrich	S5545 RRID:AB_477522	IHC (1:500)
antibody	goat polyclonal anti-5-HT	AbCam	ab66047 RRID:AB_1142794	IHC (1:500), 2% BSA in PBS blocking solution)
antibody	goat polyclonal anti-MSH	EMD Millipore	AB5087 RRID:AB_91683	IHC (1:500), 2% BSA in PBS blocking solution)
antibody	rabbit polyclonal anti-AGRP	Phoenix Pharmaceuticals	H-003-53 RRID:AB_2313908	IHC (1:500)
antibody	rabbit polyclonal anti-MCH	Phoenix Pharmaceuticals	H-070-47 RRID:AB_10013632	IHC (1:500)
antibody	rabbit polyclonal anti-CART	Phoenix Pharmaceuticals	55-102 RRID:AB_2313614	IHC (1:500)
antibody	rabbit polyclonal anti-NPY	Immunostar	22940 RRID:AB_2307354	IHC (1:500)
antibody	mouse monoclonal anti-TH	Immunostar	22941 RRID:AB_1624244	IHC (1:500)
chemical compound, drug	DiD' solid (lipid dye)	Thermo Fisher Scientific	D-7757	Stock solution (10mg/ml), working solution (2.5mg/ml), in ethanol

Fish husbandry and transgenic lines

Larvae and adults were raised in facility water and maintained on a 14:10 hr light:dark cycle at

28°C. All protocols and procedures involving zebrafish were approved by the Harvard University/Faculty of Arts & Sciences Standing Committee on the Use of Animals in Research and Teaching (IACUC). WIK wildtype larvae and mit1fa-/- (nacre) larvae in the AB background, raised at a density of ~40 fish per 10 cm petri dish, were used for behavioral and MAP-mapping experiments.

Transgenic lines *Tg(UAS-E1b:NTR-mCherry)*(Davison et al., 2007) (referred to as UAS:nfsb-mCherry), *Tg(UAS:GCaMPHS)* and *Tg(UAS:GCaMP6s)*(Muto and Kawakami, 2011; Muto et al., 2017), *Tg(HuC:GCaMP6s)*(Kim et al., 2017), *Tg(Vglut2a:dsRed)* (Miyasaka et al., 2009), *Tg(Gad1b:loxP-dsRed-loxP-GFP* and *Tg(Gad1b:GFP)* (Satou et al., 2013), *Tg(TH2:GCamP5)* (McPherson et al., 2016), *Tg(ETvmat2:GFP)* (referred to as VMAT:GFP) (Wen et al., 2008), *Tg(HCRT:RFP)* (Liu et al., 2015) have all been previously described and characterized. *Tg(pGal4FF:116A)* (referred to as 116A:Gal4) was isolated from a gene trap screen by the Kawakami group (Kawakami et al., 2010); *Tg(pGal4FF:76A)* was recently published by the same group(Muto et al., 2017). *Tg(y333:Gal4)* from a different enhancer trap screen was used to drive expression in the cH in cases where 116A:Gal4-driven expression was sparse (Marquart et al., 2015). *Tg(UAS:ReaChR-RFP)* was generated by Chao-Tsung Yang (Ahrens lab, Janelia Research Campus) using Tol2 transgenesis. The same optogenetic channel was previously validated in zebrafish in Dunn et al., 2016.

MAP-mapping of appetite regions

More details on the MAP-mapping procedure can be found in Randlett et al (2015). 5-6 dpf, *mit1fa-/-* (nacre) larvae in the AB background larvae were fed an excess of paramecia once daily. On the day of the experiment (at 7dpf), the larvae were distributed randomly into two treatment groups: 1) FOOD-DEPRIVED, where larvae were transferred into a clean petri dish of facility water, taking care to rinse out all remaining paramecia or 2) FED, where after washing and transferring they were fed again with an excess of paramecia. After two hours, larvae in both groups were fed with paramecia. After 15 minutes, larvae were quickly funneled through a fine-mesh sieve, and the sieve was then immediately dropped into ice-cold 4% paraformaldehyde (PFA) in PBS (PH 7.2-7.4). Fish were then immunostained with procedures as reported below (see Immunostaining methods). The rabbit anti-pERK antibody (Cell Signaling, #4370) and mouse anti-ERK (p44/42 MAPK (Erk1/2) (L34F12) (Cell Signaling, #4696) were used at a 1:500 dilution. Secondary antibodies conjugated with alexa-fluorophores (Life Technologies) were diluted 1:500. For imaging, fish were mounted dorsal-up in 2% (w/v) low melting agarose in PBS (Invitrogen) and imaged at ~0.8/0.8/2 µm voxel size (x/y/z) using an upright confocal microscope (Olympus FV1000), using a 20x 1.0NA water dipping objective. All fish to be analyzed in a MAP-Mapping experiment were mounted together on a single imaging dish, and imaged in a single run, alternating between treatment groups.

Whole-mount Immunostaining

24 hours after fixation (4% paraformaldehyde (PFA) in PBS), fish were washed in PBS + 0.25% Triton (PBT), incubated in 150mM Tris-HCl at pH 9 for 15 min at 70°C (antigen retrieval),

washed in PBT, permeabilized in 0.05% Trypsin-EDTA for 45 min on ice, washed in PBT, blocked in blocking solution (10% Goat Serum, 0.3% Triton in BSS or 2% BSA in PBS, 0.3% Triton) for at least an hour and then incubated in primary and secondary antibodies for up to 3 days at 4°C diluted in blocking solution. In-between primary and secondary antibodies, fish were washed in PBT and blocked for an hour. If necessary, pigmented embryos were bleached for 5 min after fixation with a 5%KOH/3%H2O2 solution.

The protocol was similar for dissected brains, except that the brains were dissected in PBS after 24 hours of fixation, and the Tris-HCL antigen retrieval/permeabilization step in Trypsin-EDTA was omitted. Dissected brains were mounted ventral up on slides in 70% glycerol prior to imaging. Confocal images of dissected brains were obtained using either a Zeiss LSM 700 or Olympus FV1000.

Quantification of 5-HT overlap with transgenic lines

The same individual manually quantified overlap of all transgenic lines with whole-mount or dissected 5-HT staining, to maintain standardization.

Quantification of food intake

Paramecia cultures (~1-2 500 ml bottles) were harvested, spun down gently (<3000 rpm) and concentrated, and subsequently incubated with lipid dye (DiD' solid, D-7757, Thermo Fisher Scientific, dissolved in ethanol) for > 2 hrs (5 µl of 2.5mg/ml working solution per 1 ml of concentrated paramecia) on a rotator with mild agitation. They were then spun down gently (<3000 rpm), rinsed and reconstituted in deionized water. An equal amount (100µl, ~500 paramecia) was pipetted into each 10 cm dish of larvae. This method was adapted from Shimada et al., 2012. After the experiment, larvae were fixed and mounted on their sides on glass slides or placed in wells of a 96 well plate. They were then imaged using the AxioZoom V16 (Zeiss) and analyzed using custom Fiji software (Schindelin et al., 2012). In cases where identity of larvae needed to be maintained, for example, to correlate food intake with brain activity, larvae were imaged and subsequently stained individually in 96 well plates. This led to more variable staining which precludes analysis of mean fluorescence.

Larvae were always distributed randomly into experimental groups.

Quantification of LH and cH activity in dissected brains

Brains within each dataset were usually registered onto a selected reference image from the same dataset using the same CMTK registration software used in MAP-mapping. Further analysis was then performed using custom Fiji and MATLAB software.

For quantification of cH, mLH and pERK fluorescence intensity, ROIs were manually defined using the reference image, and pERK intensity was quantified over all registered images and averaged across the entire lobe (multiple z-planes) as well as across both lobes. Analysis of cH

pERK fluorescence was restricted to the most ventral planes, as more dorsal cH neurons show weaker correlation with feeding states (as seen in Figure 2 – Figure Supplement 4).

For quantification of mLH and lLH active cell count, automated analysis of cell count was again performed using custom Fiji software, namely: 1) Image processing to reduce background and enhance contrast 2) Adaptive thresholding to isolate strongly-stained cells 3) Applying the "Analyze Particles" function to quantify the number of cells within each manually-defined ROI.

Aggregation and visualization of results was performed using custom MATLAB software.

Note that, in experiments in which the data was collected without the tERK channel (e.g. from Figure 2), thus prohibiting image registration, ROIs were drawn manually over each region across all z-planes and averaged to obtain mean fluorescence values.
For Figure 2 - Figure Supplement 1, where individual fish were stained, all measurements, including cell count, were made manually. In addition, background fluorescence was measured for each sample and subtracted from measured values.

Calcium imaging

For confocal calcium imaging of the cH and LH simultaneously in the presence of food, *Tg(76A:Gal4;116A:Gal4; UAS:GCaMP6s)* triple transgenic fish were embedded in 1.8% agarose, with their eyes/nostrils were released. GCaMP activity from a single z-plane (where the cH and LH neurons could be seen) was imaged using a confocal microscope (Olympus FV1000) at 1 fps. After a 5 min habituation period and a 10 min baseline period, a dense drop of paramecia was pipetted into the dish. Due to paramecia phototaxis, most of the paramecia moved into close vicinity of the fish's head under the laser, allowing for strong visual/olfactory exposure to paramecia. After image registration (TurboReg Fiji Plugin, Thevenaz et al., 1998), and downsampling (Fiji/MATLAB), manually-segmented ROIs were selected and total fluorescence within the ROI was calculated. Cross-correlation and other analyses were performed using custom MATLAB software.

For confocal calcium imaging of the caudal hypothalamus (Figure 2- Figure Supplement 3), 4 to 6 food-deprived (2-6 hrs) or fed larvae expressing *Tg(116A:Gal4; UAS:GCaMPHS)*, were embedded in 1.5% agarose on a large petri dish, and a z-stack covering the entire caudal hypothalamus imaged using multi-area time lapse imaging every 5 minutes for 2 hrs. Maximum projection images from the timelapse series were aligned to the first image of the series and total fluorescence of both caudal hypothalamic nuclei was subsequently measured using manually-drawn ROIs in ImageJ, to obtain the average calcium activity for each fish at each time point.

For 2P imaging of the cH and LH simultaneously in the absence of food (Figure 2 - Figure Supplement 4-5), *Tg(76A:Gal4;116A:Gal4; UAS:GCaMP6s)* triple transgenic fish were embedded in 1.8% agarose. GCaMP activity from either multiple slices (3 z-planes spanning a ~20 µm volume of the intermediate hypothalamus using an electrically-tunable liquid lens

(Edmund Optics, 83-922), 237 ms per z-plane) or a single z-plane where the cH and LH neurons (1.5 fps) could be seen was imaged using custom 2P microscopes. After image registration and downsampling to cell-sized voxels (Fiji/MATLAB), manually segmented ROIs were selected and total fluorescence within the ROI was calculated. Clustering, spike detection and other analyses were again performed using custom MATLAB software.

Optogenetic stimulation and simultaneous calcium imaging

Optogenetic stimulation and calcium imaging was performed on a confocal microscope (Zeiss LSM 880) using a 633 nm laser for ReaChR activation, and a 488 nm laser for calcium imaging. *Tg(y333:Gal4;UASReaChR-RFP; HuCGCaMP6s)* triple-transgenic fish were used to record LH activity after ReaChR activation. As *Tg(HuC:GCaMP6)* does not label the cH, in some cases we used fish that also had *Tg(UAS:GCaMP6s)* co-expressed in cH, allowing for monitoring of cH activity directly.

The ReaChR activation spectrum is wide and 488 nm laser power at sufficiently high intensities is sufficient to activate ReaChR. Since *Tg(y333:Gal4;UASGCaMP6s)* is expressed strongly in the cH, weak 488 nm laser power can be used to monitor cH activity after ReaChR activation of cH. On the other hand, *Tg(HuC:GCaMP6s)* expression in the LH is considerably weaker than *Tg(UAS:GCaMP6s)* expression driven by *Tg(y333:Gal4)*, and recording LH activity requires high laser power. Thus, during LH recording trials, we could not simultaneously image the cH.

Fed fish were embedded in 1.8%-2% agarose, with tails, mouth and eyes freed, 15-20 minutes before imaging in the absence of food. For baseline recording, spontaneous activities in cH or LH were recorded. ReachR activation was then induced in one side of cH periodically for 10-15 s, and ensuing activity in one or both sides of LH or cH was recorded continuously during intervals (of 120-180s) between stimuli.

Nitroreductase-mediated ablations

Larvae expressing *Tg(116A:Gal4;UAS:nfsb-mCherry)*, or their non-transgenic siblings were incubated in 2.5mM Metronidazole (Sigma-Aldrich, M3761) from 4-6 dpf/5-7 dpf. MTZ was subsequently washed out, and food intake was measured at 7 or 8 dpf. For these experiments, the MTZ-treated siblings were used as the control group. Each control or ablated group was food-deprived or fed for 2 hrs, and labeled food was added to quantify food intake. In the case of fed fish, unlabeled food was very gently washed out 15 mins before the experiment and the food-deprived fish were also agitated slightly to simulate a short washout.

Optogenetic stimulation with behavior

Optogenetic stimulation was done by placing a square LED panel (630 nm, 0.12mW/mm^2 driven at full current, Soda Vision, Singapore) directly on top of petri dishes containing ReaChR positive or negative fish, for 10 minutes continuously before or during feeding. We had attempted other methods of stimulating the fish (e.g. pulsed LED stimulation) but found that it

was disruptive to behavior.

Artemia Hunting Video

7 dpf larval fish were food-deprived for 2 hours, acclimatized in 24 well plates for 30 minutes, and then fed either an excess of hatched artemia or paramecia. Raw videos of hunting behavior were then recorded for 10 min at 30 fps using a high-resolution monochrome camera (Basler acA4924) and custom Python-based acquisition software.

High-resolution behavioral tracking

We developed a system (Johnson et al., 2019) in which a high-speed infrared camera moves on motorized rails to automatically track a zebrafish larvae in a large pool (300 x 300 x 4mm). A single fish is recruited to the arena center with motion cues delivered from a projector to initiate each trial. Paramecia are dispersed throughout the middle of the pool For analysis 60 Hz image frames are centered and aligned. In every frame, the tail was skeletonized and the gaze angle of each eye is calculated. The eyes can each move from around zero degrees (parallel to body-axis) to 40 degrees (converged for hunting). Each bout was then represented as a point in 220-dimensional posture space by accumulating 22 posture measurements (20 tail tangent angles to encode tail shape, and 2 eye gaze angles) across 10 image frames (~167 ms) from the beginning of each bout. All bouts were then mapped to a 2-D space with t-distributed stochastic neighbor embedding (t-SNE), Four major hunting bout types can be identified from this embedding. Hunts begin with the “j-turn”, and fish follow and advance toward prey objects with “pursuit” bouts. Hunts end with an “abort” or a “strike”. When the fish is not actively involved in a hunt, it explores the arena with “exploratory” bouts. Fractions of hunting bouts were then compared between fed and food-deprived fish in 3-minute time bins over 45 min.

Statistics

All error bars show mean ± SEM over fish. Significance was reported as follows: *p<0.05. Significance was determined using the non-parametric Wilcoxon Sign Rank test for paired data and the Wilcoxon rank Sum test for independent samples. One-tail tests were performed in cases where there was a prior prediction regarding the direction of change. A one-or two-way ANOVA (Tukey-Kramer correction, MATLAB statistical toolbox) was used in cases where multiple comparisons were involved.

ACKNOWLEDGEMENTS

We thank Harold Burgess kindly provided us with the y333:Gal4 transgenic line. We further thank Thomas Panier who assisted Robert Johnson in construction of the rig used for high resolution behavioral imaging. Support from Steve Turney and the CBS imaging facility, and the Harvard Center for Biological Imaging were essential for the successful completion of many experiments. Finally, we would like to thank Jessica Miller, Steve Zimmerman, Karen Hurley and Brittany Hughes at Harvard for providing invaluable fish care.

COMPETING INTERESTS

The authors declare no competing interests.

REFERENCES

Ahima, R.S., and Antwi, D.A. (2008). Brain regulation of appetite and satiety. Endocrinol. Metab. Clin. North Am. *37*, 811–823.

Ammar, A.A., Södersten, P., and Johnson, A.E. (2001). Locus coeruleus noradrenergic lesions attenuate intraoral intake. Neuroreport *12*, 3095–3099.

ANAND, B.K., and BROBECK, J.R. (1951). Hypothalamic control of food intake in rats and cats. Yale J. Biol. Med. *24*, 123–140.

Berthoud, H.-R. (2002). Multiple neural systems controlling food intake and body weight. Neurosci. Biobehav. Rev. *26*, 393–428.

Betley, J.N., Xu, S., Cao, Z.F.H., Gong, R., Magnus, C.J., Yu, Y., and Sternson, S.M. (2015). Neurons for hunger and thirst transmit a negative-valence teaching signal. Nature *521*, 180–185.

Bianco, I.H., and Engert, F. (2015). Visuomotor Transformations Underlying Hunting Behavior in Zebrafish. Curr. Biol. *25*, 831–846.

Bianco, I.H., Kampff, A.R., and Engert, F. (2011). Prey capture behavior evoked by simple visual stimuli in larval zebrafish. Front. Syst. Neurosci. *5*, 101.

BROBECK, J.R., LARSSON, S., and REYES, E. (1956). A study of the electrical activity of the hypothalamic feeding mechanism. J. Physiol. *132*, 358–364.

Chen, Y., Lin, Y.-C., Kuo, T.-W., and Knight, Z.A. (2015). Sensory Detection of Food Rapidly Modulates Arcuate Feeding Circuits. Cell *160*, 829–841.

Davison, J.M., Akitake, C.M., Goll, M.G., Rhee, J.M., Gosse, N., Baier, H., Halpern, M.E., Leach, S.D., and Parsons, M.J. (2007). Transactivation from Gal4-VP16 transgenic insertions for tissue-specific cell labeling and ablation in zebrafish. Dev. Biol. *304*, 811–824.

DELGADO, J.M.R., and ANAND, B.K. (1953). Increase of food intake induced by electrical stimulation of the lateral hypothalamus. Am. J. Physiol. *172*, 162–168.

Demski, L.S. (1973). Feeding and aggressive behavior evoked by hypothalamic stimulation in a cichlid fish. Comp. Biochem. Physiol. Part A Physiol. *44*, 685–692.

Demski, L.S., and Knigge, K.M. (1971). The telencephalon and hypothalamus of the bluegill (Lepomis macrochirus): evoked feeding, aggressive and reproductive behavior with representative frontal sections. J. Comp. Neurol. *143*, 1–16.

Dietrich, M.O., Zimmer, M.R., Bober, J., and Horvath, T.L. (2015). Hypothalamic Agrp neurons drive stereotypic behaviors beyond feeding. Cell *160*, 1222–1232.

Dockray, G.J. (2009). The versatility of the vagus. Physiol. Behav. *97*, 531–536.

Dunn, T.W., Mu, Y., Narayan, S., Randlett, O., Naumann, E.A., Yang, C.-T., Schier, A.F., Freeman, J., Engert, F., and Ahrens, M.B. (2016). Brain-wide mapping of neural activity controlling zebrafish exploratory locomotion. Elife *5*.

Elipot, Y., Hinaux, H., Callebert, J., and Rétaux, S. (2013). Evolutionary shift from fighting to foraging in blind cavefish through changes in the serotonin network. Curr. Biol. *23*, 1–10.

Filosa, A., Barker, A.J., Dal Maschio, M., and Baier, H. (2016). Feeding State Modulates Behavioral Choice and Processing of Prey Stimuli in the Zebrafish Tectum. Neuron *90*, 596–608.

Gaspar, P., and Lillesaar, C. (2012). Probing the diversity of serotonin neurons. Philos. Trans. R. Soc. Lond. B. Biol. Sci. *367*, 2382–2394.

Hoebel, B.G. (1965). Hypothalamic Lesions by Electrocauterization: Disinhibition of Feeding and Self-Stimulation. Science *149*, 452–453.

Jennings, J.H., Ung, R.L., Resendez, S.L., Stamatakis, A.M., Taylor, J.G., Huang, J., Veleta, K., Kantak, P.A., Aita, M., Shilling-Scrivo, K., et al. (2015). Visualizing Hypothalamic Network Dynamics for Appetitive and Consummatory Behaviors. Cell *160*, 516–527.

Johnson, R.E., Linderman, S., Panier, T., Wee, C.L., Song, E., Herrera, K.J., Miller, A., and Engert, F. (2019). Probabilistic Models of Larval Zebrafish Behavior: Structure on Many Scales. bioRxiv 672246.

Jordi, J., Guggiana-Nilo, D., Soucy, E., Song, E.Y., Wee, C.L., and Engert, F. (2015). A high-throughput assay for quantifying appetite and digestive dynamics. Am. J. Physiol. Regul. Integr. Comp. Physiol. ajpregu.00225.2015.

Jordi, J., Guggiana-Nilo, D., Bolton, A.D., Prabha, S., Ballotti, K., Herrera, K., Rennekamp, A.J., Peterson, R.T., Lutz, T.A., and Engert, F. (2018). High-throughput screening for selective appetite modulators: A multibehavioral and translational drug discovery strategy. Sci. Adv. *4*, eaav1966.

Kantak, K.M., Wayner, M.J., and Stein, J.M. (1978). Effects of various periods of food deprivation on serotonin turnover in the lateral hypothalamus. Pharmacol. Biochem. Behav. *9*, 529–534.

Kaslin, J., and Panula, P. (2001). Comparative anatomy of the histaminergic and other aminergic systems in zebrafish (Danio rerio). J. Comp. Neurol. *440*, 342–377.

Kawakami, K., Abe, G., Asada, T., Asakawa, K., Fukuda, R., Ito, A., Lal, P., Mouri, N., Muto, A., Suster, M.L., et al. (2010). zTrap: zebrafish gene trap and enhancer trap database. BMC Dev. Biol. *10*, 105.

Kim, D.H., Kim, J., Marques, J.C., Grama, A., Hildebrand, D.G.C., Gu, W., Li, J.M., and Robson, D.N. (2017). Pan-neuronal calcium imaging with cellular resolution in freely swimming zebrafish. Nat. Methods.

Krasne, F.B. (1962). General Disruption Resulting from Electrical Stimulus of Ventromedial Hypothalamus. Science *138*, 822–823.

Lillesaar, C. (2011). The serotonergic system in fish. J. Chem. Neuroanat. *41*, 294–308.

Lin, J.Y., Knutsen, P.M., Muller, A., Kleinfeld, D., and Tsien, R.Y. (2013). ReaChR: a red-shifted variant of channelrhodopsin enables deep transcranial optogenetic excitation. Nat. Neurosci. *16*, 1499–1508.

Liu, J., Merkle, F.T., Gandhi, A. V, Gagnon, J.A., Woods, I.G., Chiu, C.N., Shimogori, T., Schier, A.F., and Prober, D.A. (2015). Evolutionarily conserved regulation of hypocretin neuron specification by Lhx9. Development *142*, 1113–1124.

Mandelblat-Cerf, Y., Ramesh, R.N., Burgess, C.R., Patella, P., Yang, Z., Lowell, B.B., and Andermann, M.L. (2015). Arcuate hypothalamic AgRP and putative POMC neurons show opposite changes in spiking across multiple timescales. Elife *4*, e07122.

Marquart, G.D., Tabor, K.M., Brown, M., Strykowski, J.L., Varshney, G.K., LaFave, M.C., Mueller, T., Burgess, S.M., Higashijima, S., and Burgess, H.A. (2015). A 3D Searchable Database of Transgenic Zebrafish Gal4 and Cre Lines for Functional Neuroanatomy Studies. Front. Neural Circuits *9*, 78.

McPherson, A.D., Barrios, J.P., Luks-Morgan, S.J., Manfredi, J.P., Bonkowsky, J.L., Douglass, A.D., and Dorsky, R.I. (2016). Motor Behavior Mediated by Continuously Generated Dopaminergic Neurons in the Zebrafish Hypothalamus Recovers after Cell Ablation. Curr. Biol. *26*, 263–269.

Mickelsen, L.E., Bolisetty, M., Chimileski, B.R., Fujita, A., Beltrami, E.J., Costanzo, J.T., Naparstek, J.R., Robson, P., and Jackson, A.C. (2019). Single-cell transcriptomic analysis of the lateral hypothalamic area reveals molecularly distinct populations of inhibitory and excitatory neurons. Nat. Neurosci. *22*, 642–656.

Miyasaka, N., Morimoto, K., Tsubokawa, T., Higashijima, S., Okamoto, H., and Yoshihara, Y. (2009). From the olfactory bulb to higher brain centers: genetic visualization of secondary olfactory pathways in zebrafish. J. Neurosci. *29*, 4756–4767.

1187 Muto, A., and Kawakami, K. (2011). Imaging functional neural circuits in zebrafish with a new
1188 GCaMP and the Gal4FF-UAS system. Commun. Integr. Biol. *4*, 566–568.
1189 Muto, A., Lal, P., Ailani, D., Abe, G., Itoh, M., and Kawakami, K. (2017). Activation of the
1190 hypothalamic feeding centre upon visual prey detection. Nat. Commun. *8*, 15029.
1191 Pérez, M.R., Pellegrini, E., Cano-Nicolau, J., Gueguen, M.-M., Menouer-Le Guillou, D., Merot,
1192 Y., Vaillant, C., Somoza, G.M., and Kah, O. (2013). Relationships between radial glial
1193 progenitors and 5-HT neurons in the paraventricular organ of adult zebrafish - potential effects
1194 of serotonin on adult neurogenesis. Eur. J. Neurosci. *38*, 3292–3301.
1195 Pollock, J.D., and Rowland, N. (1981). Peripherally administered serotonin decreases food
1196 intake in rats. Pharmacol. Biochem. Behav. *15*, 179–183.
1197 Randlett, O., Wee, C.L., Naumann, E.A., Nnaemeka, O., Schoppik, D., Fitzgerald, J.E.,
1198 Portugues, R., Lacoste, A.M.B., Riegler, C., Engert, F., et al. (2015). Whole-brain activity
1199 mapping onto a zebrafish brain atlas. Nat. Methods *12*, 1039–1046.
1200 Satou, C., Kimura, Y., Hirata, H., Suster, M.L., Kawakami, K., and Higashijima, S. (2013).
1201 Transgenic tools to characterize neuronal properties of discrete populations of zebrafish
1202 neurons. Development *140*, 3927–3931.
1203 Schindelin, J., Arganda-Carreras, I., Frise, E., Kaynig, V., Longair, M., Pietzsch, T., Preibisch,
1204 S., Rueden, C., Saalfeld, S., Schmid, B., et al. (2012). Fiji: an open-source platform for
1205 biological-image analysis. Nat. Methods *9*, 676–682.
1206 Semmelhack, J.L., Donovan, J.C., Thiele, T.R., Kuehn, E., Laurell, E., and Baier, H. (2015). A
1207 dedicated visual pathway for prey detection in larval zebrafish. Elife *4*.
1208 Shimada, Y., Hirano, M., Nishimura, Y., and Tanaka, T. (2012). A high-throughput fluorescence-
1209 based assay system for appetite-regulating gene and drug screening. PLoS One *7*, e52549.
1210 Sternson, S.M., and Eiselt, A.-K. (2017). Three Pillars for the Neural Control of Appetite. Annu.
1211 Rev. Physiol. *79*, 401–423.
1212 Stuber, G.D., and Wise, R.A. (2016). Lateral hypothalamic circuits for feeding and reward. Nat.
1213 Neurosci. *19*, 198–205.
1214 TEITELBAUM, P., and EPSTEIN, A.N. (1962). The lateral hypothalamic syndrome: recovery of
1215 feeding and drinking after lateral hypothalamic lesions. Psychol. Rev. *69*, 74–90.
1216 Thevenaz, P., Ruttimann, U.E., and Unser, M. (1998). A pyramid approach to subpixel
1217 registration based on intensity. IEEE Trans. Image Process. *7*, 27–41.
1218 Trivedi, C.A., and Bollmann, J.H. (2013). Visually driven chaining of elementary swim patterns
1219 into a goal-directed motor sequence: a virtual reality study of zebrafish prey capture. Front.
1220 Neural Circuits *7*, 86.
1221 Voigt, J.-P., and Fink, H. (2015). Serotonin controlling feeding and satiety. Behav. Brain Res.
1222 *277*, 14–31.
1223 Watts, A.G. (2000). Understanding the neural control of ingestive behaviors: helping to separate
1224 cause from effect with dehydration-associated anorexia. Horm. Behav. *37*, 261–283.
1225 Wen, L., Wei, W., Gu, W., Huang, P., Ren, X., Zhang, Z., Zhu, Z., Lin, S., and Zhang, B. (2008).
1226 Visualization of monoaminergic neurons and neurotoxicity of MPTP in live transgenic zebrafish.
1227 Dev. Biol. *314*, 84–92.
1228 Zhu, J.-N., and Wang, J.-J. (2008). The cerebellum in feeding control: possible function and
1229 mechanism. Cell. Mol. Neurobiol. *28*, 469–478.
1230
1231
1232